J Neurophysiol 93: 2073–2089, 2005.
First published December 8, 2004; doi:10.1152/jn.00373.2004.

Impact of Time-Dependent Changes in Spine Density and Spine Shape on the Input–Output Properties of a Dendritic Branch: A Computational Study

D. W. Verzi,[1] M. B. Rheuben,[2] and S. M. Baer[3]

[1]*Department of Mathematics, San Diego State University–Imperial Valley Campus, Calexico, California;* [2]*Department of Pathobiology and Diagnostic Investigation, Michigan State University, East Lansing, Michigan; and* [3]*Department of Mathematics and Statistics, Arizona State University, Tempe, Arizona*

Submitted 12 April 2004; accepted in final form 24 November 2004

Verzi, D. W., M. B. Rheuben, and S. M. Baer. Impact of time-dependent changes in spine density and spine shape on the input–output properties of a dendritic branch: a computational study. *J Neurophysiol* 93: 2073–2089, 2005. First published December 8, 2004; doi:10.1152/jn.00373.2004. Populations of dendritic spines can change in number and shape quite rapidly as a result of synaptic activity. Here, we explore the consequences of such changes on the input–output properties of a dendritic branch. We consider two models: one for activity-dependent spine densities and the other for calcium-mediated spine-stem restructuring. In the activity-dependent density model we find that for repetitive synaptic input to passive spines, changes in spine density remain local to the input site. For excitable spines, the spine density increases both inside and outside the input region. When the spine stem resistances are relatively high, the transition to higher dendritic output is abrupt; when low, the rate of increase is gradual and resembles long-term potentiation. In the second model, spine density is held constant, but the stem dimensions are allowed to change as a result of stimulation-induced calcium influxes. The model is formulated so that a moderate amount of synaptic activation results in spine stem elongation, whereas high levels of activation result in stem shortening. Under these conditions, passive spines receiving modest stimulation progressively increase their spine stem resistance and head potentials, but little change occurs in the dendritic output. For excitable spines, modest stimulation frequencies cause a lengthening of both stimulated and neighboring spines and the stimulus eventually propagates. High-frequency stimulation that causes spines to shorten in the stimulated region decreases the amplitude of the dendritic output slightly or drastically, depending on initial spine densities and stem resistances.

INTRODUCTION

The innate properties of the dendritic trees of neurons within the CNS are highly variable and allow a wide range of functions. Some are very spiny and some are not; some conduct action potentials and some rely on electrotonic spread of input to the soma and the axon. Some, like inhibitory interneurons, are specialized to receive input quickly and to conduct action potentials at extraordinarily high frequencies with sustained depolarization, from 200 to 500 Hz (Jonas et al. 2004). Dendritic action potentials can be generated by voltage-gated calcium channels (Helmchen et al. 1999; Magee and Johnston 1995) and/or by voltage-gated sodium channels (Golding and Spruston 1998; Huguenard et al. 1989; Jung et al. 1997), and even in systems in which dendritic action potentials do not occur, voltage-gated channels modify the shapes of subthreshold synaptic potentials (Gonzalez-Burgos and Barrionuevo 2001). The density of voltage-gated channels in dendritic membranes is not necessarily uniform. Sodium channels and A-type potassium channels can be activated and distributed more densely near the postsynaptic specializations (Alonso and Widmer 1997; Frick et al. 2004; Hanson et al. 2004), which enhances the likelihood of spiking. This diversity and precise distribution of channel types allows for the different capabilities needed in the nervous system.

For many years investigators have engaged the problem of identifying the features of neuronal networks that are capable of changing in response to input from the periphery, and that could underlie learning. This search has resulted in many activity-dependent mechanisms that are invoked to varying degrees in different networks. Changes both in molecular properties of dendritic membranes and in overall structure and number of dendritic spines have been seen.

Increases in spine density can be observed in conjunction with increased synaptic activation associated with early development, increased electrical activity arising from block of inhibition, increased sensory input, providing more complex environments, or experimental induction of long-term potentiation (LTP) (Annis et al. 1994; Engert and Bonhoeffer 1999; Knott et al. 2002; Maletic-Savatic et al. 1999; Toni et al. 1999) and others reviewed by Nimchinsky et al. (2002). It has been suggested that spines may not increase in number by a splitting mechanism but rather by the emergence of dendritic protrusions (Harris et al. 2003). Decreases in spine density are observed in association with decreases in activity with block of sodium channels, deafferentation, developmental "pruning," or sensory deprivation, but may also occur after high levels of activity—excitotoxicity such as seizures, stimulation resulting in excessive glutamate release, or application of kainic acid (Müller et al. 2000; Nimchinsky et al. 2002; Oliva et al. 2002).

Direct observation of living spines with fluorescent probes has allowed us to see that their shapes can change with remarkable rapidity, within seconds (Fischer et al. 1998; Kaech et al. 2001; Krucker et al. 2000). Growth and movement of filopodia or spines can occur within minutes, either as a developmental phenomenon (Dailey and Smith 1996) or as a result of stimulation (Engert and Bonhoeffer 1999; Maletic-Savatic et al. 1999). Several studies suggest that modest activation of glutamate receptors, which gives rise to a small influx of calcium, and possibly release of calcium from internal

Address for reprint requests and other correspondence: S. M. Baer, Department of Mathematics and Statistics, Arizona State University, Tempe, AZ 85287 (E-mail: baer@math.la.asu.edu).

The costs of publication of this article were defrayed in part by the payment of page charges. The article must therefore be hereby marked "*advertisement*" in accordance with 18 U.S.C. Section 1734 solely to indicate this fact.

stores, favors lengthening of spines, but excessive stimulation and concomitant large increases in calcium cause retraction or collapse of spines (Halpain et al. 1998; Korkotian and Segal 1998, 1999; Segal et al. 2000; see review in Nimchinsky et al. 2002).

Changes in spine shape will certainly affect the spine's cytoplasmic environment as a result of increased or decreased degrees of compartmentalization. However, changes in the electrical signals of both affected and neighboring spines will also occur. Simulations show that it may be advantageous, at least if action potential conduction is the goal, for the dendrite to cluster and isolate some of the voltage-gated channels to the spine head (Baer and Rinzel 1991; Segev and Rall 1988; Tsay and Yuste 2002), so changes in the degree of synaptic isolation stemming from shape changes will have significant impact.

In this study we have focused on simulating the output of a generalized dendritic segment if morphological properties of the spines are presumed to change in some of the ways that have been observed in various systems. We considered the impact of time-dependent changes in spine density and spine shape on the properties of a dendritic branch under conditions in which the entire dendrite was assumed to have passive membrane properties, and under conditions in which voltage-gated sodium channels were clustered in the spine head. Both modest and excitotoxic levels of stimulation were explored.

METHODS

We formulate two mathematical models: the first is a model for activity-dependent spine densities and the second for calcium-mediated restructuring of individual spines. Both models are built on a continuum formulation for the interaction of many spines (Baer and Rinzel 1991).

Consider a passive dendritic cable of length l (μm), with both ends sealed, studded with a population of dendritic spines. The spine density $\bar{N}$ is defined as the number of spines per unit physical length. Over a short segment Δx, the spines deliver current $\Delta x \bar{N} I_{ss}$ to the dendrite, where I_{ss} represents the current flowing through an individual spine stem. The stem current (I_{ss}) is expressed as an I · R voltage drop across the spine stem resistance R_{ss} (MΩ), given by

$$I_{ss} = \frac{V_{sh} - V_d}{R_{ss}} \tag{1}$$

where V_{sh} and V_d (mV) are the membrane potential in the head and dendritic base, respectively. The spine stem is modeled as in previous studies (Baer and Rinzel 1991; Segev and Rall 1988) as a lumped ohmic resistor, neglecting the stem's membrane and cable properties. If the potential in the spine head is larger than the potential in the dendritic shaft ($V_{sh} > V_d$), then $I_{ss} > 0$ and the current is flowing from spine head to spine base. Conversely, if the potential in the base is larger than the potential in the head ($V_d > V_{sh}$), then $I_{ss} < 0$ and the current flow is from base to head. If $I_{ss} = 0$, then no current is passing through the spine stem.

The electrical potential $V_d(x, t)$ in a passive dendrite studded with $\bar{N}$ spines per unit physical length satisfies the cable equation

$$\pi d C_m \frac{\partial V_d}{\partial t} = \frac{\pi d^2}{4R_i}\frac{\partial^2 V_d}{\partial x^2} - \frac{\pi d V_d}{R_m} + \bar{N} I_{ss} R_m \tag{2}$$

Here R_i ($\Omega \cdot$ cm) is the specific cytoplasmic resistivity; R_m ($\Omega \cdot$ cm^2) is the resistance across a unit area of passive membrane; C_m (μF/cm^2) is the specific membrane capacitance; and d (μm) is the diameter of the dendrite. The dendrite is thought of as a distal branch. Parameter values for the cable are identified in Table 1.

TABLE 1. *Base parameter values*

Symbol	Base Value	Parameter
A_{sh}	1.31/ μm^2	Surface area of each spine head
C_{crit}	300 nM	Critical intraspine calcium level
C_m	1 μF/cm^2	Specific membrane capacitance
C_{min}	5 nM	Calcium lower bound
d	0.36 μm	Dendritic cable diameter
$\tau_{\bar{n}}$	1250 ms	Time constant for spine density
ε_1	3×10^{-3} ms^{-1}	Rate of change in C_a equation
ε_2	7.5×10^{-5} ms^{-1}	Rate of change in R_{ss} equation
γ	2.5	Channel density scale factor
l	540 μm	Physical length of the cable
L	3	Dimensionless length of the cable
$\bar{g}_{Na}$	120 mS/cm^2	Maximal sodium conductance
$\bar{g}_K$	36 mS/cm^2	Maximal potassium conductance
$\bar{g}_L$	0.3 mS/cm^2	Maximal leakage conductance
g_p	0.074 nS	Peak synaptic conductance
κ_d	1 pA	Scale factor (density model)
κ_c	0.33 pA · ms/nM	Scale factor (calcium model)
$\bar{n}_d$	18 (1 spine/10 μm)	Initial spine density (density model)
$\bar{n}_c$	25 (1–2 spines/10 μm)	Spine density for calcium model
$\bar{n}_{max}$	100 (5–6 spines/10 μm)	Spine density upper bound
$\bar{n}_{min}$	0	Spine density lower bound
R_i	70 $\Omega \cdot$ cm	Specific cytoplasmic resistivity
R_m	2500 $\Omega \cdot$ cm^2	Passive membrane resistance
R_{max}	2000 MΩ	Stem resistance upper bound
R_{min}	90 MΩ	Stem resistance lower bound
R_{sh}	1.02×10^{11} Ω	Resistance of each spine head
t_p	0.2 ms	Time to peak for g_{syn}
V_{Na}	115 mV	Sodium reversal potential
V_K	−12 mV	Potassium reversal potential
V_L	10.5989 mV	Leakage reversal potential
V_{syn}	100 mV	Synaptic reversal potential

Following Baer and Rinzel (1991), it is convenient to rewrite the cable equation in terms of dimensionless (electrotonic) length. After multiplying through by $R_m/(\pi d)$, we substitute into *Eq. 2* the membrane time constant $\tau_m = R_m C_m$, the length constant $\lambda = \sqrt{(R_m d/4R_i)}$, and the cable input resistance $R_\infty = R_m/(\pi\lambda d)$, and introduce the change of variables $X = x/\lambda$, $\bar{n} = \lambda\bar{N}$ to arrive at the (dimensionless) cable equation for electrical potential in a dendrite of dimensionless length $L = l/\lambda$

$$\tau_m \frac{\partial V_d}{\partial t} = \frac{\partial^2 V_d}{\partial X^2} - V_d + R_\infty \bar{n} I_{ss} \tag{3}$$

Here, $\bar{n}$ represents the number of spines over length λ (or number of spines per unit electrotonic length; denoted here by spines/e.l.). It is assumed throughout this paper that both ends of the dendrite are sealed, with a uniform resting potential of zero in the cable and the spine heads.

We modeled the spine head as an isopotential compartment with surface area A_{sh} (μm^2) and specific membrane capacitance C_m (μF/cm^2); individual spines have a capacitance of $C_{sh} = A_{sh} C_m$ (μF). An equation for the membrane potential in a single spine is obtained from a current balance relation for the capacitive, ionic, spine stem, and synaptic currents given by

$$C_{sh} \frac{\partial V_{sh}}{\partial t} = -I_{ion} - I_{syn} - I_{ss} \tag{4}$$

The term I_{ion} represents ionic currents passing through the head membrane and I_{syn} represents synaptic current. If the membrane is passive, then $I_{ion} = V_{sh}/R_{sh}$, where R_{sh} is the membrane resistance of the head. When modeling excitable membrane in the spine heads, we used Hodgkin–Huxley kinetics (Hodgkin and Huxley 1952) for voltage-dependent ion channel currents

$$I_{ion} = \gamma A_{sh}[(V_{sh} - V_{Na})\bar{g}_{Na}m^3h + (V_{sh} - V_K)\bar{g}_K n^4 + (V_{sh} - V_L)g_L] \quad (5)$$

Here, $\bar{g}_i$ and V_i are maximal conductances and reversal potentials, respectively, for sodium, potassium, and leakage currents. We followed Baer and Rinzel (1991) and used, except where noted, increased channel densities ($\gamma = 2.5$) and a temperature of 22°C; this corresponds to approximately 328 sodium channels per spine head. For the dendritic geometry defined here, this corresponds to $1.6\bar{n}$ channels/μm if the channels were moved from the spines to the dendritic shaft. For example, a density of 54 spines/e.l. corresponds to 86 sodium channels/μm^2 and a density of 100 corresponds to 160 sodium channels/μm^2, and so forth.

In the continuum description, we can prescribe different distributions of spines and different synaptic input patterns. However, the spine density can vary significantly with X. We simulate the activation of a cluster of synapses by applying to all spines in the activation region, $X_0 \leq X \leq X_0 + \Delta X$

$$I_{syn}(X, t) = g_{syn}(X, t)(V_{sh} - V_{syn}) \quad (6)$$

where V_{syn} is the synaptic reversal potential and g_{syn} is a brief synaptic conductance generated by the α-function

$$g_{syn}(X, t) = g_p \frac{t}{t_p} e^{[1-(t/t_p)]} \quad (7)$$

which reaches a peak synaptic conductance g_p, t_p ms after activation. *Equations 6* and *7* model a typical synaptic current observed in experiments and are similar to the equations for synaptic current used in other models. Kinetic and physical parameter values for spine heads and ionic and synaptic currents may be found in Table 1.

The synaptic input $I_{syn}(X, t)$, given by *Eqs. 6* and *7*, is applied in all simulations to the spine heads over the region $0 \leq X \leq 0.2$ periodically with g_{syn} peaking at $t_p = 0.2$ ms into each activation period, allowing the system to return to rest between activations. A graph of I_{syn} during 6 ms of an initial activation cycle for passive spines is compared with spine head potential response over the same time frame in Fig. 1. We define activation cycle as the total length of time from the beginning of a simulated synaptic input up to the beginning of the next. It is comparable to the stimulus interval. Note that the synaptic current I_{syn} peaks at about $t_p = 0.2$ ms, and returns to rest before $t = 2$ ms. The head potential (V_{sh}) for spines under synaptic activation, although slower, has fallen to 0.23 mV at $t = 6$ ms, which is close to rest. We apply no shorter than a 10-ms activation cycle to avoid affects of summation of the input. In the sections considering calcium-mediated restructuring, while g_p and t_p remain unchanged, we apply different activation frequencies; the duration of activation cycles in those sections may be found in the figures.

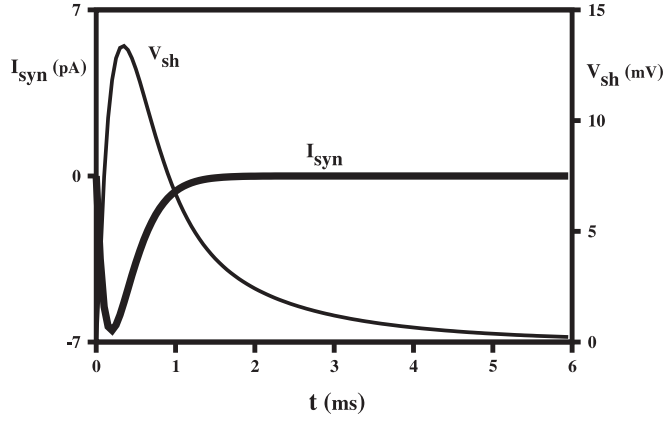

FIG. 1. Both synaptic current I_{syn} and spine head potential V_{sh} return to rest within one activation period. For passive spines the time course for I_{syn} (see *Eqs. 6* and *7*) is compared with the time course of the postsynaptic V_{sh}. Synaptic current returns to rest after 2 ms, whereas the head potential approaches rest after 6 ms. The figure illustrates that a 10 ms period between synaptic inputs is sufficient for the system to return to rest.

Model for activity-dependent density

It is convenient to use the spine stem current (I_{ss}) as a measure, over long periods of time (minutes to hours), of the electrical activity between the spine head and dendritic base (Kuske and Baer 2002; Wu and Baer 1998). Herein we explored the effects of having this electrical interaction control the local recruitment of new spines and synapses (see Fig. 2, *A* and *B*), and the loss of existing ones over time.

Let $\bar{n}(X, t)$, the spine density (number of spines per unit electrotonic length), be a dynamic variable that changes slowly in time and is dependent on electrical interactions between the spine head and the dendritic base, as measured by the spine stem current (*Eq. 1*). In general, we assume that $\partial\bar{n}/\partial t$ is proportional to I_{ss}. If $I_{ss} > 0$ then $\bar{n}$ increases, and decreases when $I_{ss} < 0$. Furthermore, we assume that the spine density changes slowly in time, on a scale much slower than a single synaptic event.

A continuum model for activity-dependent spine densities is

$$\tau_m \frac{\partial V_d}{\partial t} = \frac{\partial^2 V_d}{\partial X^2} - V_d + R_\infty \bar{n} I_{ss} \quad 0 < X < L,\ t > 0 \quad (8)$$

$$C_{sh} \frac{\partial V_{sh}}{\partial t} = -I_{ion} - I_{syn} - I_{ss} \quad (9)$$

$$\tau_{\bar{n}} \frac{\partial \bar{n}}{\partial t} = (I_{ss}/\kappa_d)(1 - \bar{n}/\bar{n}_{max})(\bar{n} - \bar{n}_{min}) \quad (10)$$

The initial distribution of spine density, $\bar{n}_d$, the maximum and minimum spine density parameters, $\bar{n}_{max}$ and $\bar{n}_{min}$, which bound $\bar{n}$, are given in Table 1. Note that if $I_{ss} = 0$, $\bar{n}$ is constant in time, but could still be spatially nonuniform.

The system of *Eqs. 8–10* is nonlinear because *Eq. 10* is nonlinear. This is true even if the membrane properties of the spine heads and cable are assumed to be passive. However, $\bar{n}$ changes slowly because $\tau_{\bar{n}}$ is at least 3 orders of magnitude larger than the membrane time constants for the spine heads and dendrite (e.g., $\tau_m = 2.5$ ms and $\tau_{\bar{n}} =$ 1,250 ms). For the passive membrane case, *Eqs. 8* and *9* constitute a linear subsystem that acts on a fast time scale (milliseconds), and *Eq. 10* for $\bar{n}$ is a single equation acting on a slow time scale (seconds). Changes in spine density depend on changes in I_{ss}, which in turn depend on the integrative properties of the surrounding membrane and synaptic activity. This formulation does not require $\bar{n}$ to be continuous in space (X).

In most of our simulations for this model, the synaptic input will be repeated every 10 ms, a period short enough to capture the dynamics of V_{sh} and V_d but long enough to allow those potentials to return to resting values. The spine density appears constant on a 10-ms time scale. The spine density's dynamics are resolved on the time scale of $\tau_{\bar{n}}$ (on the order of seconds in our simulations). Increasing $\tau_{\bar{n}}$ slows down the change in spine density. In an earlier variation of the model (Verzi 2000) the effect of varying $\epsilon = 1/\tau_{\bar{n}}$ was explored. It was found that there exists ϵ^* such that for $\epsilon < \epsilon^*$ the dynamical properties of the system remain invariant. In this paper, a sufficiently large value of $\tau_{\bar{n}}$ was chosen that was biologically plausible and computationally efficient. To integrate the system we used a semi-implicit Crank–Nicholson (for *Eq. 8*) and Adams–Bashforth (for time integration) finite-difference method. This method is sufficiently fast without sacrificing the accuracy of computations.

Model for calcium-mediated restructuring

Although activity affects—and is affected by—the distribution and density of spines along the dendrite, so also are the structures of individual spines. Recent experiments implicate the intraspine calcium level as a mediator for changes in dendritic spine structure

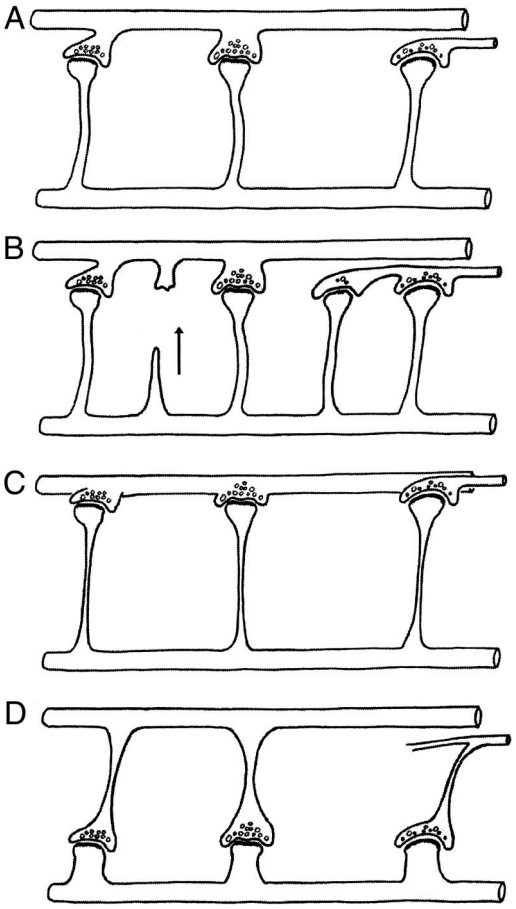

FIG. 2. Simulated morphological changes. *A*: starting point for each of the simulations is a number of evenly spaced spines with similar spine stem shapes. *B*: a subset of these spines at a particular location will receive synaptic input. In the first series of simulations, we examine the situation in which the dendrite receiving input responds to that activity by growing new spines in response to the current flows that are generated; a local increase in spine density is thereby created. *C*: in the second series of simulations, synaptic activity causes a proportionate increase in cytoplasmic calcium. If the increase in calcium ions is small, the spine stems elongate and become thinner, thus increasing spine stem resistance. *D*: if the influx of calcium is large, greater than a "threshold" amount, the spine stems collapse into the dendrite. We assume that the presynaptic axonal processes are plastic, and that the synaptic connection is not terminated by change in spine stem shape.

(reviewed in Nimchinsky et al. 2002). Spines of cultured hippocampal neurons have been monitored over several hours (Korkotian and Segal 1999). Release of calcium from internal stores, in response to pulse applications of caffeine, induced a small transient rise in Ca^{2+} (200–400 nM), and an increase in the length of spine stems in <5 min. Conversely, Halpain et al. (1998) induced a rapid collapse of dendritic spine stems (also within 5 min) by stimulating cultured neurons with glutamate. This caused maximal calcium influx, raising intraspine calcium to much higher levels.

A diagrammatic model has been proposed for spine restructuring based on the above experiments (Harris 1999) and is illustrated in Fig. 2, *C* and *D*. A moderate amount of synaptic activation may result in spine stem elongation. However, a high level of activity may cause too much calcium influx and induce spine stem shortening or loss, perhaps as a result of actin depolymerization. A continuum model for a uniform distribution of spines (with spine density $\bar{n}_c$ constant in time) consistent with the above hypothesis is

$$\tau_m \frac{\partial V_d}{\partial t} = \frac{\partial^2 V_d}{\partial X^2} - V_d + R_\infty \bar{n}_c I_{ss} \tag{11}$$

$$C_{sh} \frac{\partial V_{sh}}{\partial t} = -I_{ion} - I_{syn} - I_{ss} \tag{12}$$

$$\frac{\partial C_a}{\partial t} = -\varepsilon_1 (C_a - C_{min}) + |I_{ss}|/\kappa_c \tag{13}$$

$$\frac{\partial R_{ss}}{\partial t} = -\varepsilon_2 (R_{ss} - R_{min}) \left(1 - \frac{R_{ss}}{R_{max}}\right) \left(\frac{C_a}{C_{min}} - 1\right) \left(\frac{C_a}{C_{crit}} - 1\right) \tag{14}$$

In *Eq. 13*, the change in intraspine calcium C_a is dependent on activity, as measured by $|I_{ss}|$. In the absence of activity ($I_{ss} = 0$) calcium decays slowly to a minimal value, denoted by C_{min}. In *Eq. 14*, the spine stem resistance R_{ss} is a dependent variable that reflects changes in spine stem structure. The stem resistance approaches steady state in the absence of activity because C_a approaches C_{min} when $I_{ss} = 0$. An earlier mathematical formulation made the counterintuitive assumption that spines grow to their maximum length (i.e., R_{ss} approaches R_{max}) in the absence of activity (Verzi and Baer 2004). When synaptic activity is present the stem resistance approaches steady state if R_{ss} approaches R_{max} or R_{min}, or if I_{ss} drives C_a to C_{crit}.

This model builds on the simplified Wu–Baer model (Wu and Baer 1998) for a single spine with an activity-dependent stem conductance. Only here, activity-dependent calcium is viewed as a second messenger that regulates changes in spine stem resistance (reciprocal of conductance). We identify a critical intraspine calcium level, C_{crit}, that is threshold or critical to whether local spines become long and thin or short and stubby. The stem resistance increases for $C_a < C_{crit}$ (subcritical), modeling spine stem elongation, and decreases for $C_a > C_{crit}$ (supercritical), modeling spine stem shortening, as described by the Harris diagrammatic model.

The system of *Eqs. 11–14* is nonlinear because *Eq. 14* is nonlinear; *Eqs. 13* and *14* constitute a slow subsystem for variables R_{ss} and C_a. Parameter values for this model are found in Table 1 and in the figure legends. Kinetic and physical parameters for the cable and spine heads are identical to those used in the model for activity-dependent spine densities. We also assume that the dendritic cable has sealed end-boundary conditions and that the dendritic shaft and spines have zero rest potentials. The system was integrated using the semi-implicit method described earlier.

RESULTS

Activity-dependent density

We use *Eqs. 8–10* to explore the dynamics of a dendritic cable with activity-dependent spine density. Here, density is constrained to increase slowly in response to current flow toward the dendrite ($I_{ss} > 0$), as would occur with excitatory synaptic input, but decreases when current flows from dendrite to spine ($I_{ss} < 0$), as would occur in response to local potential changes or to inhibitory input. The effects of changes in spine numbers in both the presence and the absence of voltage-gated channels, and for short, low-resistance spines versus long high-resistance spines will be compared (Table 2).

ACTIVITY-DEPENDENT DENSITIES: PASSIVE SPINES. Initially 54 passive spines are uniformly distributed along a passive cable of length $L = 3$ e.l. ($\bar{n} = 18$ spines/e.l. or 1 spine/10 μm in this dendrite), with uniform spine stem resistance fixed at $R_{ss} = 1{,}240$ MΩ. Spines are synaptically activated over the region $0 \leq X \leq 0.2$ (initially 3.6 spines) every 10 ms, allowing sufficient time for the spine head potential to return to rest between activations. We examined first the projected spine density changes, and then the ultimate effects on potentials arising in spines adjacent to those stimulated, and finally on the dendritic potentials farther downstream from the stimulated site.

TABLE 2. *Summary table: stimulation related density increases*

Input Number	Number of Spines in the Synaptically Activated Region	Peak Potential in Head at $X = 0.1$ in mV	Peak Potential in Neighboring Heads, $X = 0.4$ in mV	Peak Dendritic Potential "Output" at $X = 2.0$, in mV
		Passive Spines		
$R_{ss} = 1240$ MΩ				
1	3.6	13.38	4.78	0.43
60	4.1	14.18	5.40	0.50
120	4.6	15.02	6.04	0.56
Change after 60 cycles	+1.0	+1.64	+1.26	+0.13
$R_{ss} = 100$ MΩ				
1	3.6	8.74	5.14	0.46
60	4.1	9.86	5.85	0.53
120	4.6	11.02	6.57	0.60
Change after 60 cycles	+1.0	+2.28	+1.43	+0.14
		Active Spines		
$R_{ss} = 1240$ MΩ				
1	3.6	17.20	7.29	0.51
30	4.0	37.90	36.35	1.81
60	4.3	47.64	54.14	23.74
Change after 60 cycles	+0.7	+30.44	+46.85	+23.23
$R_{ss} = 100$ MΩ				
1	3.6	8.65	4.97	0.36
60	4.2	9.80	5.69	0.41
360	7.5	47.99	41.03	6.26
480	8.6	57.52	48.51	32.40
Change after 60 cycles	+0.6	+1.15	+0.72	+0.05
Change after 480 cycles	+5.0	+48.87	+43.54	+32.04

Figure 3*A* shows the initial spine density over the cable (*left*), and the amplitude and time course for spine head potential at various points (V_{sh}, *center*) and along the dendrite (V_d, *right*) during the first 6 ms of the initial activation cycle. The location $X = 0.1$ is at the center of the synaptically activated region; $X = 0.4$ is immediately downstream from the activated region; and $X = 2.0$ is much farther downstream, where it could be considered as the "output" of the region in question.

Figure 3*B* shows that after 60 cycles of synaptic input ($t = 600$ ms), the density increases within the input region (about $\bar{n} = 20.5$ spines/e.l.), but decreases slightly to the right of the activation site. The density decrease occurs because current flows from the dendritic base toward the spine head as depolarization spreads along the dendrite from the adjacent activated spines. The greatest increase in spine density occurs near the downstream edge of the activation region ($X = 0.2$) because stem currents there have the greatest average magnitude. As the spine density increases and more spines become available for synaptic stimulation (an increase of 0.5 spines by cycle 60), the added synaptic current causes maximum spine head potential within the stimulated region to increase from 13.38 mV during cycle 1 to 14.18 mV by cycle 60. In the adjacent region, at $X = 0.4$, the amplitude in the neighboring (unstimulated) spine heads increases from 4.78 to 5.40 mV. After 120 cycles (Fig. 3*C*), the spine density in the input region increases to approximately 23.2, an increase of 4.3 spines from the initial distribution. The addition of only 1 stimulated spine causes a 1.26mV increase in peak amplitude seen in neighboring spines.

Figure 4 graphs the evolution with time of peak head and dendritic membrane potentials, and spine density, at the same 3 spatial locations as in Fig. 3, over 500 activation cycles. The increase in the synaptic potentials in the spine heads and dendritic shaft is roughly linear, especially at distances far from the input site. At $X = 2.0$ there is little or no response to the stimuli. The increase in spine density is also roughly linear at $X = 0.1$, with only a negligible change in density downstream for spines with passive membrane. The increase in spines in the stimulated region (from 3.6 to 9 spines over 500 activations), however, is sufficient to have an impact on the amplitude of the passive spread of depolarization to the neighboring spines (compare $X = 0.1$ and $X = 0.4$ in Fig. 4, *A* and *B*). On the other hand, the local increase in density by itself does not have much effect on the output of the dendrite because the resulting spread of potential down the dendrite, from this increase in synaptically activated spines, leads only to a small 0.07 mV rise in dendritic potential at $X = 2.0$.

Spine stem resistances have been estimated from morphological measurements of spine neck diameters (0.9–411 MΩ) as well as from the diffusional exchange of Ca^{2+} between dendritic spines and the shaft (4–150 MΩ) (see Harris and Stevens 1989; Svoboda 1999; Svoboda et al. 1996). If spine stem resistances are lower, the results are qualitatively similar. For 100 MΩ spines the impact on the neighboring spines is enhanced both initially and after subsequent density increases (Table 2).

ACTIVITY-DEPENDENT DENSITIES: EXCITABLE SPINES. The next series of figures considers spines with voltage-gated channels. The active membrane in the spine heads is modeled with Hodgkin–Huxley kinetics, with I_{ion} given by *Eq. 5*. We have explored both the implications of channel density and of the spine stem length on the model's predictions.

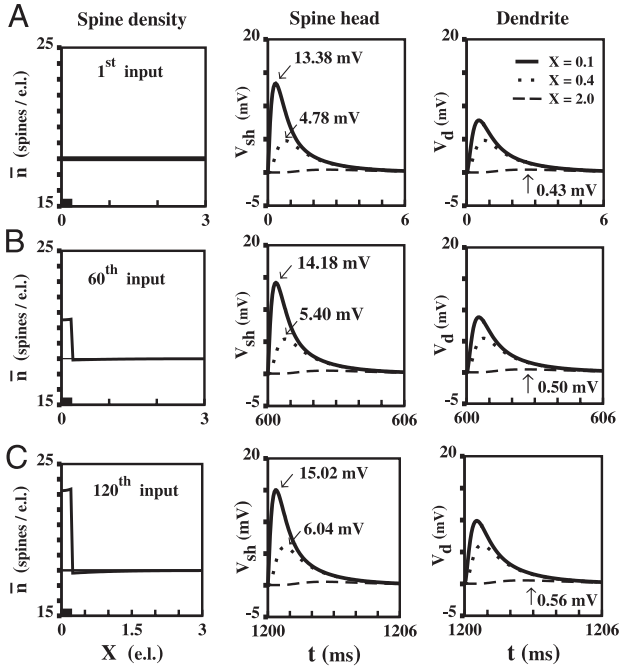

FIG. 3. Repetitive synaptic input to passive spines with activity-dependent spine densities: changes in spine density remain local to the input site. A cable of dimensionless length 3 ($\lambda = 179.3\ \mu$m) and diameter 0.36 μm, with both ends sealed, has $R_\infty = 1233\ \text{M}\Omega$. ($R_m = 2{,}500\ \Omega \cdot \text{cm}^2$, $R_i = 70\ \Omega \cdot \text{cm}$). The dendrite has a uniform distribution of 54 passive spines; spine density (number per λ) is initially $\bar{n} = 18$. Spine resistance is $R_{ss} = 1{,}240\ \text{M}\Omega$. Spines near $X = 0$ ($0 \leqslant X \leqslant 0.2$) are periodically activated every 10 ms with peak conductance 0.074 nS (region indicated by the bar), with I_{syn} given by *Eqs. 6* and *7*. *A*: initially (1st input) the spine density is uniformly distributed (*left panel*). Potentials in the head (*middle panel*) and dendrite (*right panel*) are shown for 3 spatial locations: at $X = 0.1$ in the middle of the stimulated cluster, and $X = 0.4$, and $X = 2.0$, which correspond to unstimulated regions. *B*: after 600 ms (60 inputs), and with $\kappa_d = 1$ pA and $\tau_{\bar{n}} = 1.25$ sec, the spine density at the input site increases from 18 (3–4 spines) to 20.5 (4 spines), but remains relatively constant outside the stimulus region. *C*: after 1,200 ms (120 inputs) the spine density increases to 23.2 (gaining only one more spine). Increase in density of the stimulated spines causes only a 1.26-mV increase in head potentials in the spines adjacent to the stimulated cluster, and the output of the dendrite is increased by only 0.13 mV.

In Fig. 5 the spine stem resistance, R_{ss}, is 1,240 MΩ. At the initial spine density of 18 excitable spines/e.l., no action potential is generated in the stimulated spines after a single stimulus, but the peak amplitudes in the stimulated and adjacent spines are greater as a result of the addition of voltage-gated channels (compare Fig. 3*A* to Fig. 5*A*). However, the voltage output of the dendrite is still small.

When the synaptic input is repeated every 10 ms, as in the previous section, the spine density slowly changes over time. After 30 stimuli the density within the region of stimulated spines has increased. This results in a greatly enhanced response in both the spines at the stimulation site and those immediately adjacent at $X = 0.4$ (Fig. 5*B* and Table 2).

After 60 stimuli (Fig. 5*C*), action potential generation in the spine heads extends to at least $X = 2.0$ because of density increases that reach as far as $X = 2.0$. The spines downstream are now generating their own membrane current (I_{ion}) that dominates, on average for each stimulus, the current source from the dendrite. The spines located at $X > 2.2$ have average stem currents directed the opposite way because these spines have not yet generated their own membrane current, and thus the temporary drop in density there.

The effect of simply assuming the presence of voltage-gated channels in the spine heads may be seen by comparing Fig. 5*C* with Fig. 3*C*. Spines are added to the unstimulated region as well as to the input region. The evolving density profile increases maximum spine head potential downstream at $X = 0.4$ by 46.85 mV, and the maximum dendritic potential farther downstream at $X = 2.0$ by 23.23 mV, compared with initial activation. The increase in peak head and dendritic potentials is nonlinear at all 3 spatial points (Fig. 6). The curves increase rapidly as the spine density, at the input site, crosses a threshold for the generation of an action potential. Peak head potentials at $X = 0.4$ (dotted) have greater magnitude than spine heads at $X = 0.1$ because of an increase in current flowing downstream from the cluster of spines accumulating within the input region.

In the time scale shown in Fig. 6*C*, the change in spine density appears approximately piecewise linear with the rate of increase over the input region shifting downward in response to

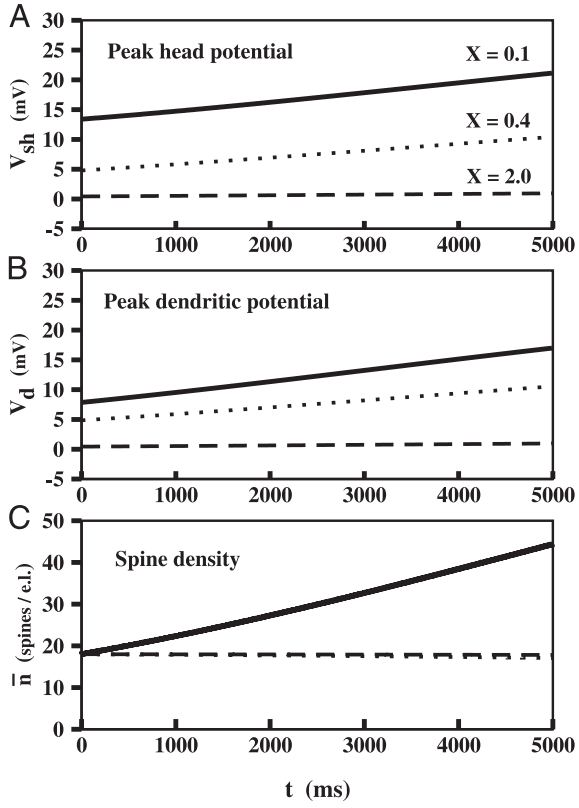

FIG. 4. Dynamic stimulus–response curve for slowly changing spine densities (passive spines). For passive spines with activity-dependent densities the peak head and dendritic potentials increase slowly and roughly linearly as the spine density increases. Same parameter values as Fig. 3. Time evolution of the peak head and dendritic membrane potential and spine density is plotted for 3 spatial locations: the middle of the input site $X = 0.1$ (solid), adjacent to the input site $X = 0.4$ (dotted), and distant from the site $X = 2.0$ (dashed). *A*: rise in peak head potential is nearly linear at all 3 spatial points along the dendrite. However, the rate of increase decreases with distance from the input site. *B*: peak dendritic potential rises linearly at approximately the same rate as the peak head potentials at the same spatial location, but with smaller peak values. *C*: after 500 inputs the spine density increases, but only in the vicinity of the input site. Number of spines at the input site increases from about 4 (at $t = 0$) to 9 (at $t = 5{,}000$ ms), but remain at about 18 spines/electrotonic length (e.l.) outside the input region.

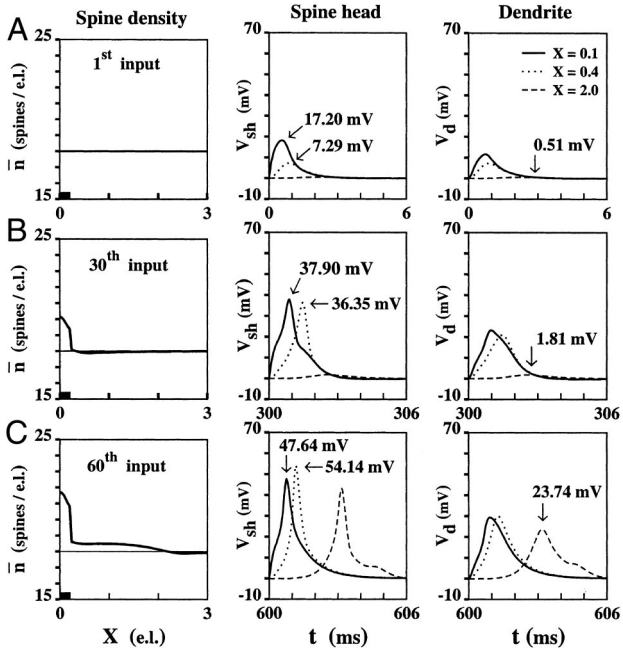

FIG. 5. Repetitive synaptic input to excitable spines with activity-dependent spine densities: spine density increases both inside and outside the input region, forging a path for impulse propagation. A passive cable, with the same geometric and electrical parameters as in Fig. 3, has an initial uniform distribution of 54 excitable spines. However, the excitable spines have Hodgkin–Huxley (HH) membrane in their spine heads; ion channel densities are $\gamma = 2.5$ HH values (HH kinetics for squid at 22°C). As in Fig. 3, the stem resistance is $R_{ss} = 1{,}240$ MΩ and spines are activated every 10 ms with a peak conductance of 0.074 nS over the input region $0 \leqslant X \leqslant 0.2$; indicated by the bars on the time axis. *A*: initially (1st input) the spine density is uniformly distributed (*left*). Postsynaptic response is subthreshold in the head (*middle*) and dendrite (*right*) as shown for 3 spatial locations. *B*: after 30 inputs, the spine density in the input region increases from 18 to just over 20, but drops slightly outside the region. This local increase in spine density is sufficient to generate a local action potential at $X = 0.1$. Impulse propagates to $X = 0.4$ but then fails. *C*: after 60 inputs the spine density increases both inside and outside the input region. Propagation is successful to $X = 2.0$, resulting in a substantial increase in the output of the dendrite at that point, from 1.81 to 23.74 mV.

the onset of spine head action potentials. At $X = 0.1$, the spine density grows more slowly when compared with the passive case (see Fig. 4*C*). Unlike the passive case, spine densities gradually increase outside the input region rather than remaining nearly constant.

When very long stimulus times are considered the spine densities at $X = 0.1$ and $X = 2.0$ are seen to asymptote to $\bar{n}_{max}$ (See Fig. 7*A*). However, at $X = 0.4$ the spine density grows at a slower rate because of its proximity to the input region. At the input region the spines generate, in unison, a large flux of current that drives current outward through adjacent spine stems. This outward current causes the adjacent spine heads to generate their own action potentials, which act as a counterbalance. The net effect is that the magnitude of the spine stem current (I_{ss}) of adjacent spines is reduced, slowing down the growth of $\bar{n}$ (see *Eq. 10*).

We next considered the influence that the density of voltage-gated channels might have on the phenomena seen above. If the sodium conductance is decreased because of a reduction in channel density, it is more difficult to generate and propagate action potentials. As a result of propagation failure, downstream spine heads generate insufficient current to dominate the influx of current entering at their base. So, $I_{ss} < 0$ and the spine density decays to $\bar{n}_{min} = 0$. This is illustrated in Fig. 7*B* for the downstream location $X = 2.0$ (dashed). The spatial profile of the spine density (*right*) shows that after a long time (40,000 cycles of input) an impulse can travel no further than $X = 1.5$ and so the spine density values for $X > 1.5$ decay to the minimum value.

There will be an interaction between the assumed density of voltage-gated channels and the spine density because jointly they determine the total number of channels. Increasing $\bar{n}_{max}$ allows more spines to be recruited, effectively increasing the density of sodium channels. In Fig. 7*C* the spine density is allowed to increase to $\bar{n}_{max} = 180$. At $X = 2.0$ (dashed) initially the spine density decays, but it eventually reverses and grows to $\bar{n}_{max}$. The reason for this initial decay is that successful action potential propagation to $X = 2.0$ required over 20,000 activation cycles (simulation not shown) compared with <60 cycles for the higher sodium conductance case (see Fig. 6). Note that even though it takes about 100 times longer to forge a pathway for propagation for the low sodium con-

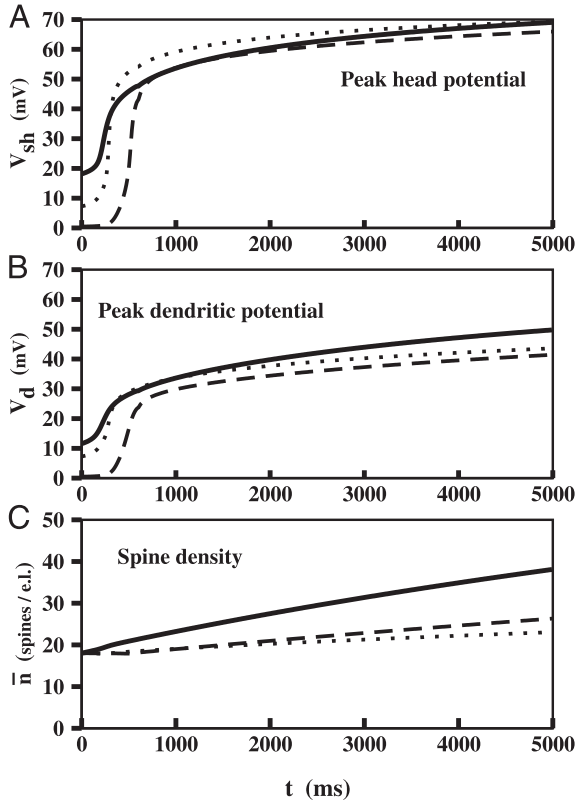

FIG. 6. Dynamic stimulus–response curve for slowly changing spine densities (excitable spines and large R_{ss}). Same parameter values as Fig. 5. Time evolution of the peak head and dendritic potentials, and spine density are plotted for $X = 0.1$ (solid), $X = 0.4$ (dotted), and $X = 2.0$ (dashed). *A*: rise in peak spine head potential is nonlinear at all 3 spatial points. Rapid increase in potential after a small number of stimuli is attributed to local action potential generation. Voltage peaks in spine heads increase to about 70 mV as the spine densities increase with time. *B*: peak dendritic potentials. After about 1,000 ms, the peak dendritic potentials at all 3 locations reach values quite close to each other, differing by <10 mV. At 5,000 ms, the output in the dendrite is near 40 mV, a significant increase considering there was little or no output to start with. *C*: spine density at $X = 0.1$ increases at a slower rate than in the passive case (compare with Fig. 4*C*). However if stimulation continues, the spine densities increase outside the input region, whereas in the passive case the densities remain nearly constant.

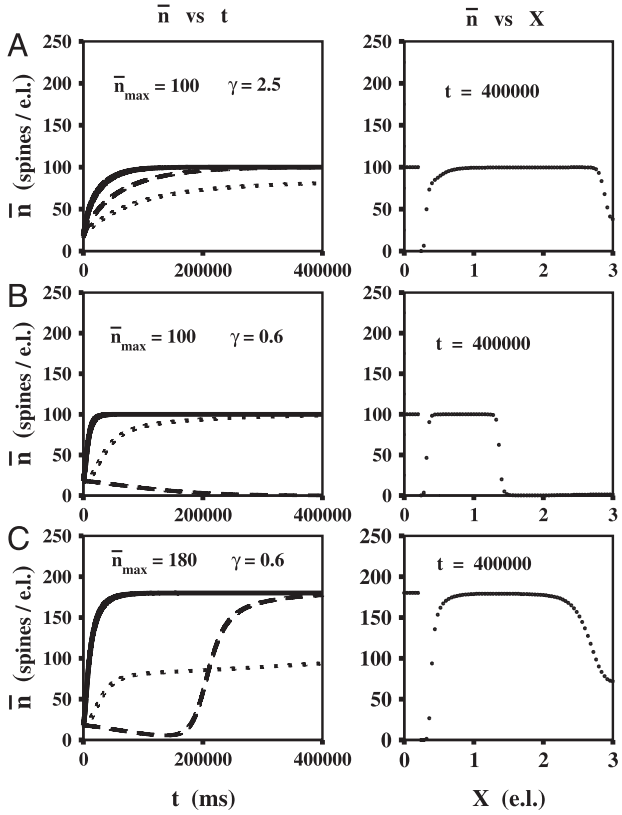

FIG. 7. Relationships between spine densities and voltage-gated channel densities. *Left panels*: long-time evolution of the spine density for $X = 0.1$ (solid), $X = 0.4$ (dotted), and $X = 2.0$ (dashed). *Right panels*: spatial profile of the spine density at 400,000 ms. *A*: long-time evolution of the spine density for the same parameters as in Fig. 5 with continuous stimulation at 10 ms intervals. Downstream from the input site the spine density approaches $\bar{n}_{max} = 100$. *B*: channel densities are reduced by changing in *Eq. 5* to $\gamma = 0.6$. This lowers the sodium conductance to 720 pS/μm^2 and the potassium conductance to 216 pS/μm^2. At the output site (*left panel*, dashed) the spin density decays to $\bar{n}_{min} = 0$. The spatial profile shows that after 40,000 input cycles the spine density has decayed to $\bar{n}_{min}$ for all points to the right of $X = 1.5$, a consequence of repetitive propagation failure near $X = 1.5$. *C*: if the maximum spine density is increased to $\bar{n}_{max} = 180$ the effectiveness of the active channels in propagating action potentials is recovered as well as the downstream growth of spines. As in *A* the spines downstream approach their maximum value $\bar{n}_{max}$.

ductance case, the shape of spine density profiles in Fig. 7, *A* and *C* are very similar at $t = 400{,}000$ ms.

In model dendrites, when the spines are postulated to have voltage-gated channels, it has been found that propagation of an action potential from spine to spine is precluded if spine stem resistance (R_{ss}) is either too large or too small. The likelihood of propagation is also affected by the density of spines along the dendrite (Baer and Rinzel 1991). The value we used for R_{ss} in Fig. 5 did not allow an action potential to propagate for the initial spine density, but promoted propagation at higher densities.

In the next series of simulations, the effect of assuming that spines have lower spine stem resistances is considered. For the channel densities giving a conductance value of $\gamma = 2.5$, if spine stem resistance is 100 MΩ, no active response occurs initially either in the stimulated spine heads or in adjacent ones for these initial conditions. The spine heads at $X = 0.1$ have a peak potential of 8.65 mV, and peak potential in the dendrite at $X = 2.0$ is negligible for the first stimulus (Fig. 8*A*).

With repeated stimulation, an increase in spine density at the activation site occurs slowly over time, as before. However, it takes a full 360 cycles of synaptic activation (Fig. 8*C*) to create a cluster adequate to generate an action potential that propagates as far as $X = 0.4$. In Fig. 8*D*, the chain of action potentials reaches farther downstream to $X = 2.0$. Activity has increased the stimulation cluster to 8.6 spines, having added 5 new spines for activation over 480 cycles of stimulation. For these lower values of R_{ss}, the difference between the dendritic and head potential is small. Spine density increases behind the propagating wave, except immediately adjacent to the stimulation cluster. It seems counterintuitive that the density drops below initial values within a region affected by a propagating

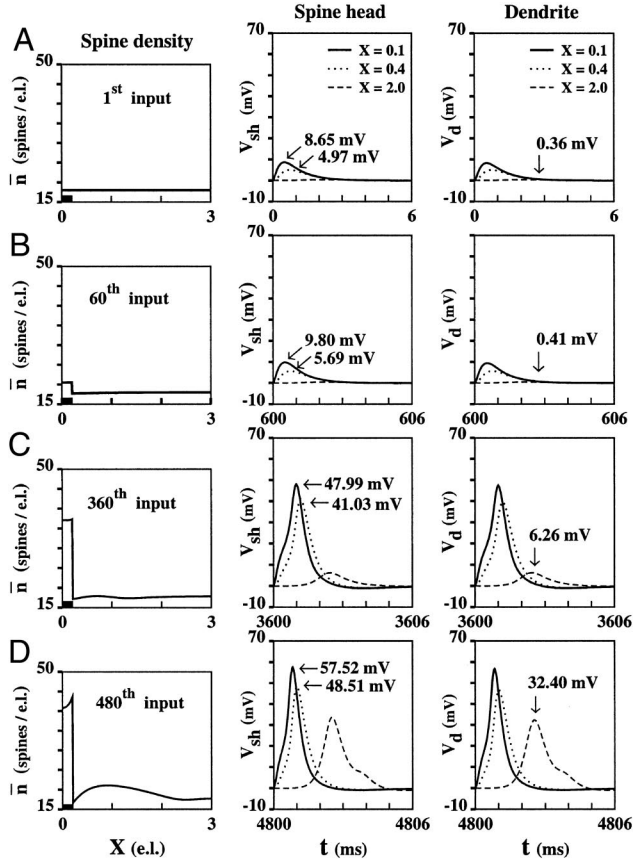

FIG. 8. Repetitive synaptic input to excitable spines with lower stem resistance. A passive cable, but with spines having excitable membranes as in Fig. 5, has an initial uniform distribution of 54 excitable spines, only now the spine stem resistances are uniformly reduced to $R_{ss} = 100$ MΩ. For this lower stem resistance the membrane potentials in the head and dendritic shaft are nearly identical. Spines are periodically activated as in Fig. 5. *A*: initially (1st input), the spine density is uniformly distributed (*left panel*). Postsynaptic response is subthreshold in the head (*middle*) and dendrite (*right*). In the dendrite, the amplitude of the potential at $X = 2.0$ is indicated (arrow). *B*: after 60 inputs, the spine density in the input region increases from 18 to just over 20, but this local increase in spine density is insufficient to generate a local action potential at $X = 0.1$ (cf. Fig. 5*B*). *C*: after 360 inputs, the spine density reaches 37 and an action potential is generated at $X = 0.1$ and propagates to $X = 0.4$, but fails before reaching $X = 2.0$. *D*: after 480 inputs, propagation reaches the target $X = 2.0$, with spine density increasing adjacent to and to the right of the input region, but decaying farther down the dendrite. Note that the peak of the action potential in the spine heads is greatest at the input site for lower values of R_{ss}. Compare with Fig. 5*C*, where it is the adjacent spines at $X = 0.4$ that have the highest peak potentials.

wave, but the stem current there is on average negative over each 10-ms cycle because the dendrite is receiving so much input from the cluster upstream.

Figure 9 plots peak head and dendritic membrane potentials, and spine density for $R_{ss} = 100$ MΩ. Spine density at the input site is higher after 3 s than for the passive case, but the rate of change in density decreases once spines reach threshold for an action potential (cf. Fig. 4). The most significant effect is that the increase in dendritic output takes longer to begin and climbs more slowly than when $R_{ss} = 1{,}240$ MΩ.

Table 2 summarizes the 4 preceding experiments for model dendrites with passive and active spines of low and high stem resistances. It can be seen that the addition of relatively small numbers of spines can have a significant effect on the peak amplitudes of potentials conducted to neighboring spines and, if the spines are presumed to contain voltage-gated channels, on the dendritic output. The particular numbers should not be construed to have any particular significance, but rather the point of the comparison is to determine the relative, and order-of-magnitude changes, in amplitude if spine densities change.

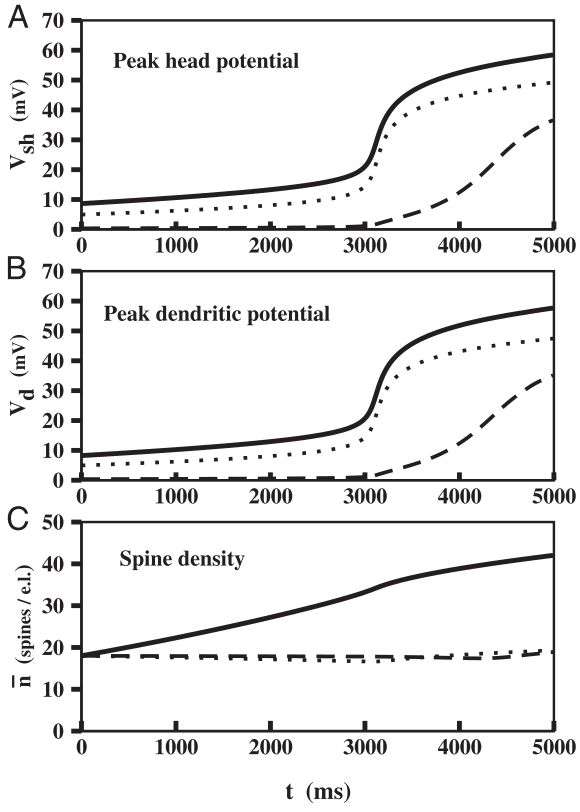

FIG. 9. Dynamic stimulus–response curve for slowly changing spine densities (excitable spines and lower R_{ss}). Same parameter values as Fig. 8. Time evolution of the peak head and dendritic potential and spine density is plotted for $X = 0.1$ (solid), $X = 0.4$ (dotted), and $X = 2.0$ (dashed). *A*: rise in peak head potential is nonlinear at all 3 spatial points but the transition to larger values occurs much later than for the large stem resistance case (cf. Fig. 6). *B*: response curve for the peak dendritic potential is nearly the same as in the head because of the low stem resistance. Although the potential in the dendrite does not increase as dramatically as in the case with higher spine stem resistances, there is a region of the curve between 3,000 and 5,000 ms that the output voltage rises quite steadily with each successive stimulus. *C*: spine density at the input site increases similarly to the passive case until the density is sufficiently large to generate an action potential. Spine density begins to increase outside the input region after propagation is initiated (between 4,000 and 5,000 ms).

Calcium-mediated spine restructuring

In the model for spine restructuring, *Eqs. 11–14*, there are 2 slow variables, R_{ss} and C_a, and the spine density is assumed constant (in time and space). We consider 75 spines uniformly distributed along a cable of electrotonic length 3 ($\bar{n}_c = 25$).

RESTRUCTURING WITH PASSIVE SPINES. For the passive spine case, $I_{ion} = V_{sh}/R_{sh}$ in *Eq. 12*, and as in previous sections we simulate the periodic activation of synapses on the spine heads over the region $0 \leqslant X \leqslant 0.2$. The frequency of activation, with the concurrent influx of Ca^{2+}, is the primary control parameter in contrast to the previous series. Figure 10 illustrates the dynamics of the model at $X = 0.1$ in response to 3 different frequencies applied to the input region. Initially, there is a uniform distribution of spines and all spines are uniform in structure (i.e., R_{ss} is constant for all X along the dendritic shaft of electrotonic length 3). At a low frequency of 5 Hz (inputs repeat every 200 ms) there is a small increase in calcium (Fig. 10*A*). This causes an increase in the stem resistance from initially 750 MΩ to just above 1,000 MΩ (Fig. 10*B*). Also note that at $t = 3{,}500$ ms, when the synaptic stimulation ceases, the stem resistance approaches steady state as calcium decreases to its minimum value.

For 50 Hz (every 20 ms) the effect is more dramatic. The calcium level at the input site reaches approximately 150 nM, which results in a significant increase in R_{ss} to nearly 2,000 MΩ. These input frequencies increase the calcium concentration only to subcritical levels (below the dashed line in Fig. 10*A* at 300 nM) corresponding to spine elongation in the Harris description. For 125 Hz, a frequency likely to occur rarely under physiological condition, calcium is driven to supercritical concentrations, which ultimately drives the stem resistance downward. Figure 10 simply reflects the paradigm that small increases in intraspine calcium cause elongation of the spine stem, whereas increases approaching a toxic level cause shortening.

For passive spines, the mathematical model predicted that calcium-mediated restructuring would remain largely local. This is illustrated in Fig. 11 for the subcritical input frequency of 50 Hz. Because the dendrite and spines have passive membrane properties, the membrane potential decreases exponentially away from the input site. This is seen in Fig. 11 by comparing peak spine head and dendritic membrane potentials at $X = 0.1$ and $X = 2.0$. For example, for each input cycle displayed, the peak potential in the heads or dendrite at $X = 2.0$ does not exceed 0.6 mV, whereas at $X = 0.1$ (middle of input region) the peak potential is about 10 mV in the dendrite and >10 mV in the heads. Also note that the time courses for the head and shaft potentials are nearly identical at $X = 0.4$ and $X = 2.0$, for each input cycle. Thus the spine stem current I_{ss}, our measure of electrical activity, is negligible away from the input region [recall $I_{ss} = (V_{sh} - V_d)/R_{ss}$]. Thus I_{ss} is near 0 in *Eq. 13*, forcing C_a to approach C_{min} outside the input region. The right side of *Eq. 14* approaches zero, which explains why R_{ss} does not change outside the input region in Fig. 11. Thus our simulations for passive spines indicate that, although a spine may restructure as a result of synaptic activation, the

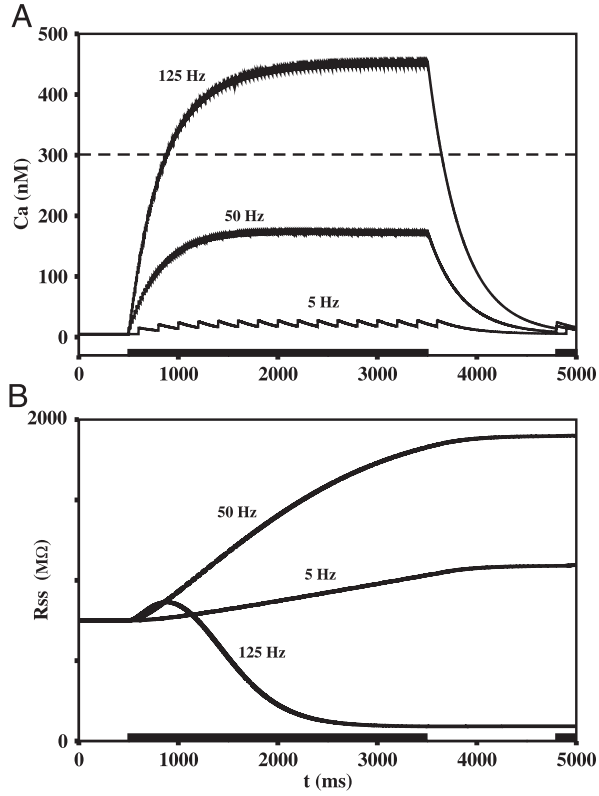

FIG. 10. Repetitive synaptic input to passive spines modifies intraspine Ca^{2+} levels, which mediate changes in spine stem resistance. A passive cable of electrotonic length 3 (with diameter and R_∞, R_m, R_i the same as in Fig. 3) has a uniform distribution of 75 passive spines ($\bar{n}_c = 25$). Unlike previous simulations, the spine density is kept constant. Initially, the spine stem resistance is $R_{ss} = 750$ MΩ for all spines. Simulations for 3 input frequencies are shown. Between 500 and 3,500 ms, and between 4,800 and 5,000 ms (indicated by the solid bars on the time axis) spines are periodically activated at 5 Hz (every 200 ms), 50 Hz (every 20 ms), and 125 Hz (every 8 ms). Peak synaptic conductance and I_{syn} are the same as in Fig. 3. *A*: calcium response in the center of the input site ($X = 0.1$) for the 3 different input frequencies. High-frequency input (125 Hz) drives C_a above the critical value of 300 nM (dashed). Calcium remains below criticality for the lower input frequencies (5 and 50 Hz). At 3,500 ms, the input is turned off and calcium returns to its resting value of 5 nM. *B*: stem resistance response to calcium concentration at the input site. Effect of the 125 Hz input is to initially increase R_{ss} (because $C_a < 300$), it then peaks at 1,000 ms, which coincides with the critical calcium value, then the resistance decreases rapidly as calcium rises above criticality and the spines collapse into the dendrite. Lower-frequency input (5 and 50 Hz) monotonically increases R_{ss}. Stem resistance rises more rapidly in response to the 50 Hz input. With cessation of activity at 3,500 ms the stem resistance continues to rise, but quickly levels out as C_a approaches its rest value.

restructuring remains in or near the input region and with little change to the electrical response of the system. The spread of potential to neighboring spines is actually decreased by increased spine stem resistance.

RESTRUCTURING WITH EXCITABLE SPINES. When voltage-gated channels are considered to be present in the spine heads, the spread of electrical activity, and subsequent calcium-based restructuring, is no longer local to the input region. In Fig. 12 the spines in the input region are activated at a frequency of 20 Hz (input every 50 ms). Initially (1st input; Fig. 12*A*) the peak head and dendritic potential are subthreshold to action potential generation. However, after 18 inputs (Fig. 12*B*), a local action potential is generated inside ($X = 0.1$) and just outside ($X = 0.4$) the input region. After the 58th input, action potentials propagate to $X = 2.0$. The spread of electrical activity down the dendritic shaft drives calcium levels upward toward C_{crit} (see Fig. 13), thereby causing R_{ss} to increase for all 75 spines (see Fig. 12*C*, *left* and Fig. 13). For channels configured in the spine heads, an increase in R_{ss} electrically isolates excitable channels, allowing them to reach threshold with less current. These simulations suggest that the presence of excitable channels in spines could promote the propagation of electrical activity, causing restructuring of dendritic spines (represented here by changes in R_{ss}) at points far from the synaptic input region. This effect is, of course, based on the starting assumption that only current flow is required for shape change. If (as might also be simulated) concurrent synaptic activity is a necessary feature, the changes would halt at the boundary of the stimulated region. Similarly, small changes in the geometry such as a region of low spine density would also halt the effect.

Having spines start with an initial low stem resistance delays but does not prevent the onset of structural and functional changes. Figures 13 and 14 are dynamic stimulus–response curves for an input frequency of 20 Hz. In Fig. 13 the initial stem resistance is 750 MΩ compared with 100 MΩ in Fig. 14. For the larger stem resistance the distal spine heads at $X = 2.0$

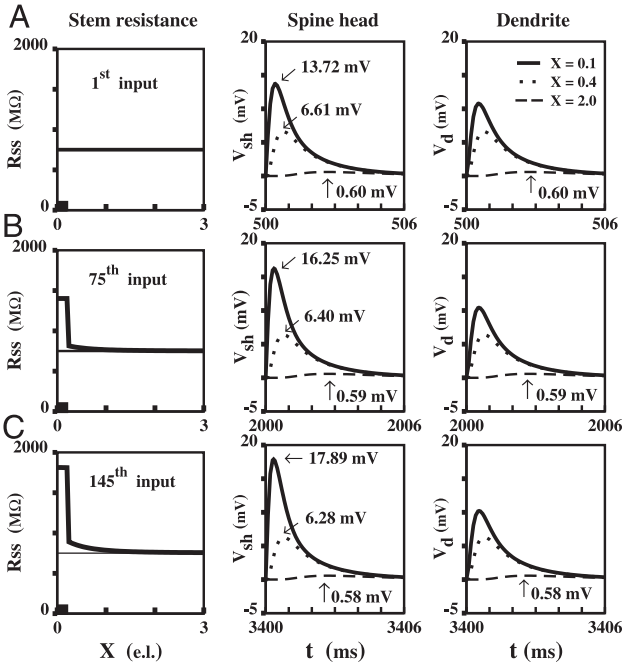

FIG. 11. Repetitive synaptic input to passive spines with calcium-mediated stem restructuring: changes in spine stem resistance remain local to input site. Passive spines on a passive cable are periodically activated at a frequency of 50 Hz (every 20 ms); all other parameters are the same as in Fig. 10. *A*: 1st input occurs at 500 ms. Stem resistance is initially 750 MΩ for all 75 spines, which are uniformly distributed over $0 < X < 3$ (*left*). Potentials in the spine head (*middle column*) and dendrite (*right column*) are shown for the middle of the stimulated region (solid: $X = 0.1$), just outside the input region (dotted: $X = 0.4$) and distal to the region (dashed: $X = 2.0$). *B*: after 2,000 ms (75 inputs) the stem resistance in the input region increases from 750 MΩ to just under 1,500 MΩ, but there is little change outside the region. In the stimulated region the peak head potential increases by almost 3 mV, and just outside the region there is a small decrease of <1 mV. There is a negligible change in dendritic potentials. *C*: after 3,400 ms (145 inputs) the rise in stem resistance remains local and the peak head potential in the stimulated region increases by another 2 mV. However, outside the input region the change in the peak head and dendritic potentials are small. There is actually a decrease in amplitude after the spine stem resistance increases in the stimulated spines.

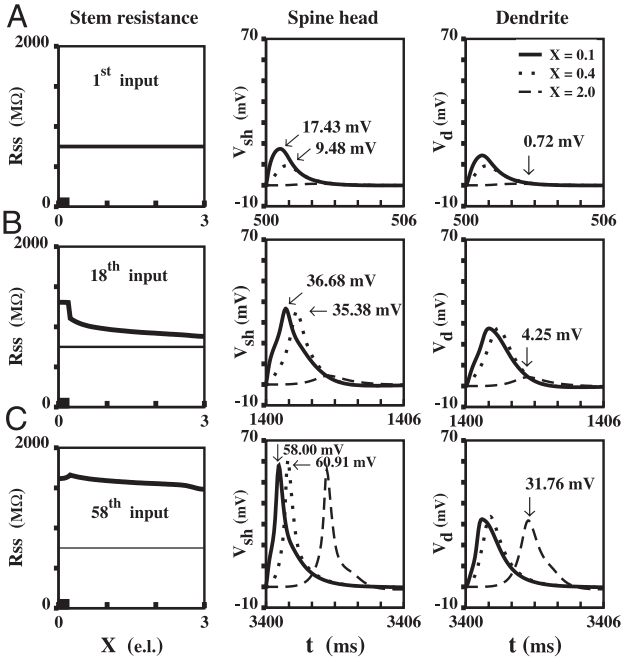

FIG. 12. Repetitive synaptic input to excitable spines with calcium-mediated stem restructuring: stem resistance increases both inside and outside the input region. Excitable spines on a passive cable are periodically activated at a frequency of 20 Hz (every 50 ms). Excitable spines have HH kinetics, as described in Fig. 5. Spines were set to have an initial stem resistance of 750 MΩ. *A*: initially (1st input at 500 ms) the stem resistance is uniform for all spines (*left*). Postsynaptic response is subthreshold in the head (*middle*) and dendrite (*right*) as shown for 3 spatial locations. *B*: after 1,400 ms (18 inputs) the stem resistance in the input region increases about 67%, and the output is increased almost 6-fold. Unlike the passive case (cf. Fig. 11) the stem resistance increases also significantly outside the input region. This increase in resistance is sufficient to generate a local enhanced potential at $X = 0.1$ that propagates to $X = 0.4$. *C*: after 3,400 ms (58 inputs), the stem resistance grows to large values inside and outside the input region. Propagation in the heads is successful to $X = 2.0$, resulting in a significant increase in output of the dendrite at that point, from 4.25 to 31.76 mV.

begin firing at 1,500 ms, which immediately affects the dendrite (Fig. 13*A*). For low initial stem resistance, firing begins just outside the input region ($X = 0.4$) at about 7,500 ms, and onset at $X = 2.0$ requires almost 20 s. Thus downstream changes in calcium and stem resistance at $X = 2.0$ are still possible if the initial spine stem resistance is low (compare Fig. 13 and Fig. 14).

Input frequencies of intermediate value are best for facilitating electrical propagation pathways. The effectiveness of 3 input frequencies are compared in Fig. 15, at $X = 0.1$ and $X = 2.0$. The figure shows that if the frequency of input is too high, say 100 Hz (10 ms period), then calcium in the input region rises above C_{crit}, driving down the stem resistances, thus precluding propagation. At the other extreme, if the frequency is too low, such as a frequency of 5 Hz (200-ms period), calcium builds up slowly, which significantly increases the time it takes for R_{ss} to grow to values great enough for action potential generation and propagation. However, as Fig. 15 illustrates, the intermediate value of 20 Hz (50 ms period) drives calcium to just below C_{crit} in the input region, which promotes an increase in the growth rate of R_{ss} and facilitates propagation. When the synaptic input ceases at $t = 3{,}500$ ms, calcium decays to its minimum value and the stem resistances corresponding to the 3 frequencies approach new distinct rest states. If the synaptic input persisted the stem resistances at $X = 0.1$ would approach the equilibrium value R_{max} for frequencies 20 and 5 Hz and R_{min} for 100 Hz.

Successful propagation depends not only on frequency but also on C_{crit}. For very high values of C_{crit} (500 nM) propagation is successful for the frequency range 5–100 Hz. Low values of C_{crit} (10 nM) preclude propagation in the preceding frequency range. For intermediate values of C_{crit} (150–450 nM) propagation is successful for lower input frequencies but not for higher frequencies.

An important question is what frequencies, if any, give rise to an equilibrium R_{ss} that is different from R_{max} or R_{min}? For $C_{crit} = 300$ nM we found that for frequencies between 20 and 80 Hz calcium settles into steady-state oscillations (over the input region) that average C_{crit}. This gives rise to steady-state R_{ss} values other than R_{max} or R_{min}.

Figure 16 shows an example for an input frequency of approximately $33\frac{1}{3}$ Hz (30 ms period). At $X = 0.1$ (Fig. 16*B*), the peak-to-peak average of calcium rises and overshoots $C_{crit} = 300$ nM but then decays back to C_{crit} through damped

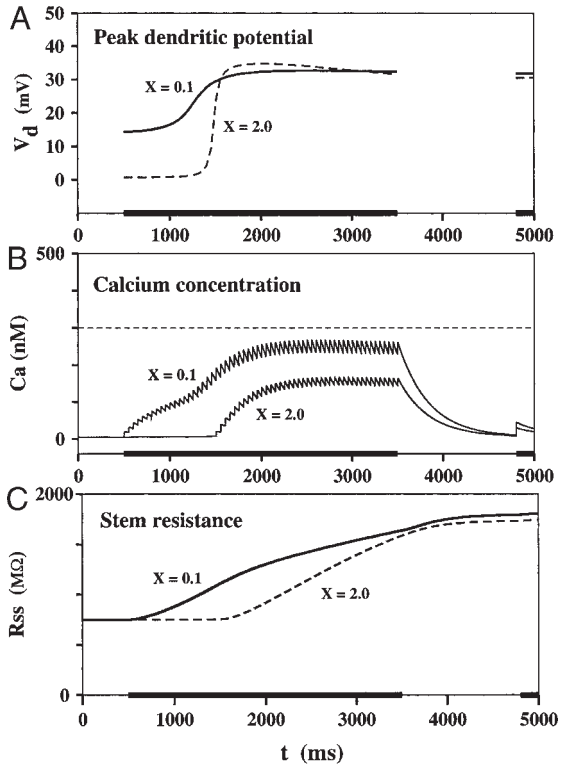

FIG. 13. Dynamic stimulus–response curve for calcium-mediated stem restructuring (excitable spines and R_{ss} initially large). Same parameters and input frequency (20 Hz) as in Fig. 12. All spines have an initial stem resistance of 750 MΩ. Time evolution of the peak dendritic potential, calcium concentration, and stem resistance is plotted for the center of the input region $X = 0.1$ and distally at $X = 2.0$. *A*: between 1,200 and 1,800 ms, the peak dendritic potentials increase rapidly in the input region and distally. At approximately $t = 1{,}500$ ms there is a sharp steplike transition for $X = 2.0$, which indicates that potentials generated in the input region are beginning to affect voltage-gated channels in spine heads in the region near $X = 2.0$. *B*: impulses propagating to $X = 2.0$ (and other distal locations) cause an increase in calcium concentration there. Although calcium concentration increases locally and distally, at this frequency of input the calcium concentration remains below its critical value (300 nM, dashed). *C*: because calcium remains below criticality, the stem resistance increases for all spines along the cable, and thereby facilitates the generation of spine head action potentials and impulse propagation.

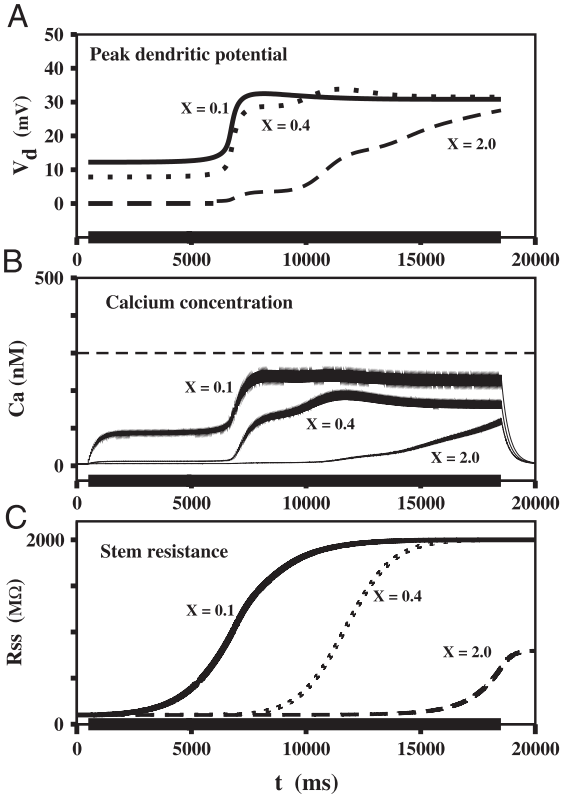

FIG. 14. Dynamic stimulus–response curve for calcium-mediated stem restructuring (excitable spines and initially lower R_{ss}). Same parameters as Fig. 13, except initially R_{ss} = 100 MΩ. Time evolution of the peak dendritic potential, calcium concentration, and stem resistance is plotted for $X = 0.1$, $X = 0.4$, and $X = 2,0$. *A*: transition to larger peak potentials occurs much later than for the case of initially large stem resistances (cf. Fig. 13). *B*: this delay arises from the slower increase in calcium concentration and stem resistance (*C*).

oscillations. We found that damped oscillations to steady state occur for frequencies 25 to 40 Hz. Between 40 and 80 Hz calcium overshoots C_{crit} and then exponentially decays to C_{crit} without oscillations. In Fig. 16*C*, the stem resistance, at $X = 0.1$, oscillates in response to the slow calcium oscillations. Eventually R_{ss} of the stimulated spines approaches a constant steady state about 50 MΩ above its initial value of 750 MΩ.

The oscillations in stem resistance give rise to amplitude modulations in dendritic spiking, as seen in Fig. 16*A*. However, these modulations decay as R_{ss} approaches steady state. This transient modulated spiking occurs over the narrow frequency range of 30–35 Hz. At 33⅓ Hz the modulated spiking at $X = 0.1$ evolves into dendritic bursting oscillations at $X = 2.0$ and then quickly decays. Figure 16*A* (dashed) shows that the initial active phase of the burst has 15 spikes. The subsequent 3 active phases decrease in amplitude and spike number. It is important to emphasize that these bursting oscillations occur over a narrow frequency range and do not persist.

Figure 17 demonstrates the effects of modeling the onset of a high-frequency "excitotoxic" synaptic input. In Fig. 17, a 20 Hz synaptic input drives the stem resistance to values that support spiking in the spine heads. The peak dendritic potential at the input and output locations plateau in the vicinity of 30 mV. At 2,500 ms the input frequency is changed to 100 Hz, which could be an excitotoxic frequency for many nerve cells. This causes a supercritical surge in intracellular calcium that drives the stem resistance down at the input site. Within 250 ms the dendritic spikes cease and the peak response drops to near 10 mV. This electrical activity is insufficient to spread downstream to distal dendritic regions, so the potential at the output site quickly approaches rest values. However, it is interesting to note that the low level of electrical activity at the target leads to a slow rise in R_{ss} there, providing those excitable spines with a lower threshold for spiking if stimulated.

Current estimates of spine stem resistance (Tsay and Yuste 2004) include values as low as 30 or 40 MΩ. Electrically, at these low resistance values, the synaptic potentials in the heads are approximately equal to the potentials in the dendritic shaft. It has been found that if low stem resistance spines are excitable and the spine density is sufficiently large, the dendritic cable behaves like an excitable axon, where action potential generation and propagation are all or none (Baer and Rinzel 1991). In Fig. 18 we simulate a dendritic cable where R_{ss} is bounded between 30 and 500 MΩ, and with a larger population of uniformly distributed spines (105 spines rather than 75 spines as in Fig. 17). At the onset of high-frequency stimulation (100 Hz), there is a supercritical surge in intracellular calcium with the associated decrease in R_{ss}, as was the case in Fig. 17. However, here the dendritic spikes do not cease

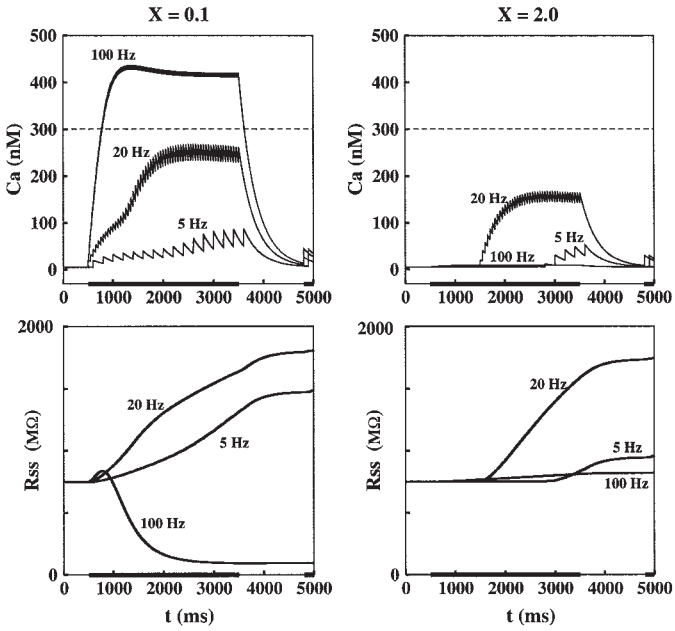

FIG. 15. Effects of low, intermediate, and high-frequency stimulation. Same parameters as Fig. 13. Initially, the stem resistance is set at R_{ss} = 750 MΩ for all spines. Simulations for 3 input frequencies are shown at $X = 0.1$ (*left*) and away from the input region at $X = 2.0$ (*right*). Input of 20 Hz (50-ms periods) used in previous simulations forges a pathway for action potential propagation in spine heads (see Figs. 12 and 13). However, a high-frequency input of 100 Hz (10 ms periods) drives the calcium concentration at the input region above criticality (*top left*), which has the effect of then reducing the stem resistance there (*bottom left*). Action potentials are more difficult to generate in spines with low stem resistance, so electrical activity remains local to the input region. Therefore at $X = 2.0$, the calcium concentration (*top right*) and stem resistance (*bottom right*) remain constant. At the other extreme of 5 Hz (200 ms periods), the calcium concentration rises slowly at $X = 0.1$, causing the stem resistance to also rise slowly. Not until near 3,000 ms does the stem resistance become large enough to propagate electrical activity away from the input region, as indicated by the late rise in calcium and stem resistance (*top and bottom right*, respectively). This formulation therefore successfully replicates a biological situation in which low-frequency stimulation makes only subtle local changes in spine properties, whereas higher-frequency trains produce enhancement in output along the branch.

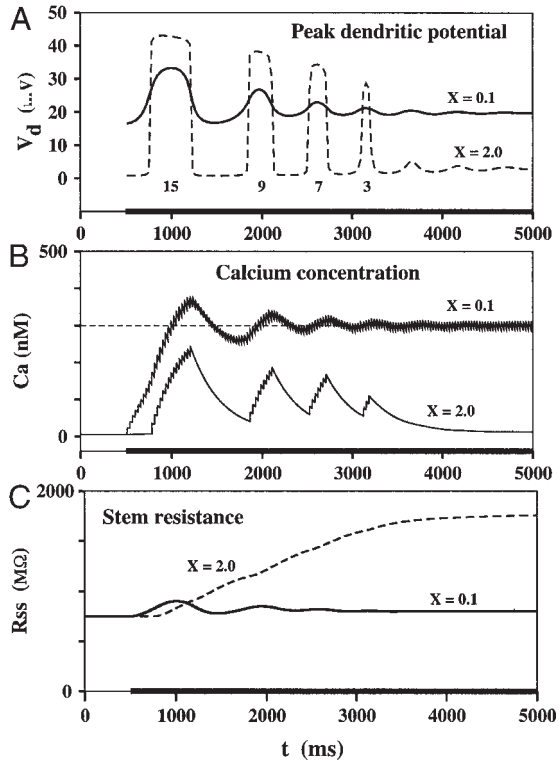

FIG. 16. Example of an input frequency in which the stem resistance approaches an equilibrium value other than R_{max} or R_{min}. Same parameters as Fig. 13 only now the input frequency is set at 33⅓ Hz (30-ms period), a value within a range of input frequencies (20–80 Hz) giving rise to equilibrium stem resistances that are not R_{max} or R_{min}. Peak dendritic potentials, calcium concentration, and stem resistances are plotted for the center of the input region $X = 0.1$ and distally at $X = 2.0$. *A*: peak dendritic potential at the input site (solid) displays damped oscillations (corresponding to damped amplitude modulations) as it approaches steady state (repetitive spiking). Distally, at $X = 2.0$ (dashed) the peak potentials are decaying square waves. Square waves correspond to bursts of spikes that decay in amplitude and frequency. Numbers 15, 9, 7, and 3 refer to the number of spikes occurring in the preceding active phase of the burst. *B*: calcium at $X = 0.1$ decays (on average) to $C_{crit} = 300$ nM (dashed line). At C_{crit}, R_{ss} is constant (see *Eq. 14*). At $X = 2.0$ the sawtooth calcium oscillations are attributed to the bursts of spikes in the dendrite and spine heads at $X = 2.0$. *C*: at $X = 0.1$, R_{ss} approaches a steady-state value of 800 MΩ (solid), demonstrating that an equilibrium stem resistance different from R_{max} or R_{min} is possible.

as the subset of spines shorten because of the larger density of active spines. In this case the short spines and their associated voltage-gated channels continue to receive input and to function, albeit with changed properties.

However, it is also biologically possible to have a situation where the high-frequency stimulation is truly excitotoxic, and causes not just spine shortening but actual spine loss (Müller et al. 1993). A simple way to incorporate spine pruning in our calcium-mediated restructuring model is by making $\bar{n}$ a dependent variable in *Eqs. 11–14* and by adding the new equation

$$\frac{\partial \bar{n}}{\partial t} = -\varepsilon_3 H(R_{ss}, C_a)(\bar{n} - \bar{n}_{min}) \tag{15}$$

where

$$H(R_{ss}, C_a) = \begin{cases} 1 & \text{if } R_{ss} < R_{ss}^* \text{ and } C_a > C_{crit} \\ 0 & \text{otherwise} \end{cases} \tag{16}$$

In this new equation, $\bar{n}$ decreases if R_{ss} is lower than R_{ss}^* and C_a is greater than C_{crit}; otherwise, $\bar{n}$ remains constant.

In Fig. 19, we rerun the simulation displayed in Fig. 18, only now with this new variation of the model. Figure 19*A* shows the spine density beginning to slowly decrease in the input region after the onset of high-frequency stimulation. The effective channel density decreases until action potential generation fails in the input region, then there is an abrupt cessation of output from the dendritic branch.

DISCUSSION

The amplitude of the output of a dendritic branch depends initially on the strength of the synaptic input (number of spines that are activated from a particular axon pathway) and then on the properties of its structure. The important factors include branch diameter, presence, location, and density of different types of voltage-gated channels, and presence and properties of spines along its length.

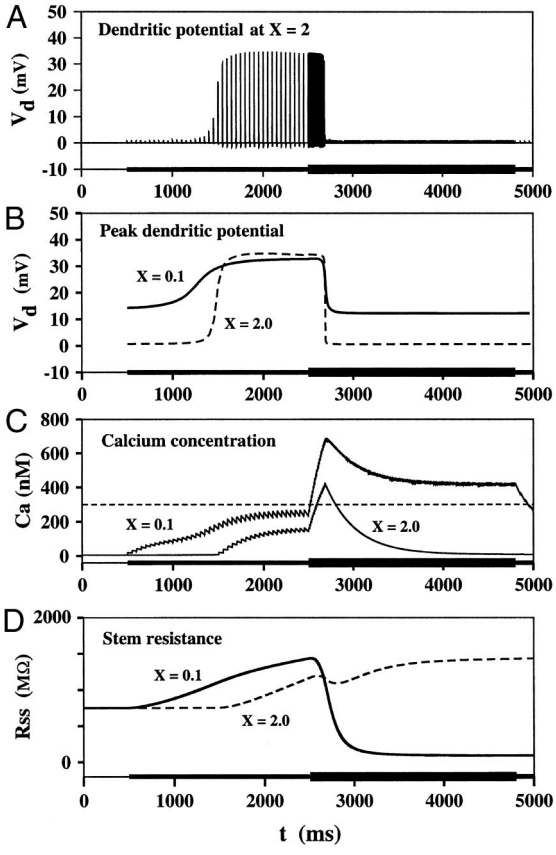

FIG. 17. Burst of high-frequency stimulation can effectively reduce dendritic output when spines shorten. Same parameters as Fig. 13. An intermediate synaptic input frequency of 20 Hz (duration indicated by thin bar on *t*-axis) is followed, at $t = 2{,}500$ ms, by a high-frequency 100 Hz input (duration indicated by thick bar). *A*: amplitude of dendritic output potentials, at $X = 2.0$, increases with intermediate stimulus but at the onset of high-frequency stimulation, the amplitude decreases to near 0 at $t = 2{,}750$ ms. *B*: peak dendritic potentials decrease abruptly shortly after the onset of high-frequency stimulation. *C*: sharp decrease in potential is associated with a surge in spine calcium concentration, which is caused by the increase in synaptic input frequency. *D*: at the input site the stem resistance decreases rapidly after the onset of high-frequency input, leading to decreases in the output because the voltage-gated channels are no longer isolated and no longer are able to generate an action potential. At the output site, $X = 2.0$, the stem resistance continues to increase as a result of subcritical calcium levels caused by low electrical activity there.

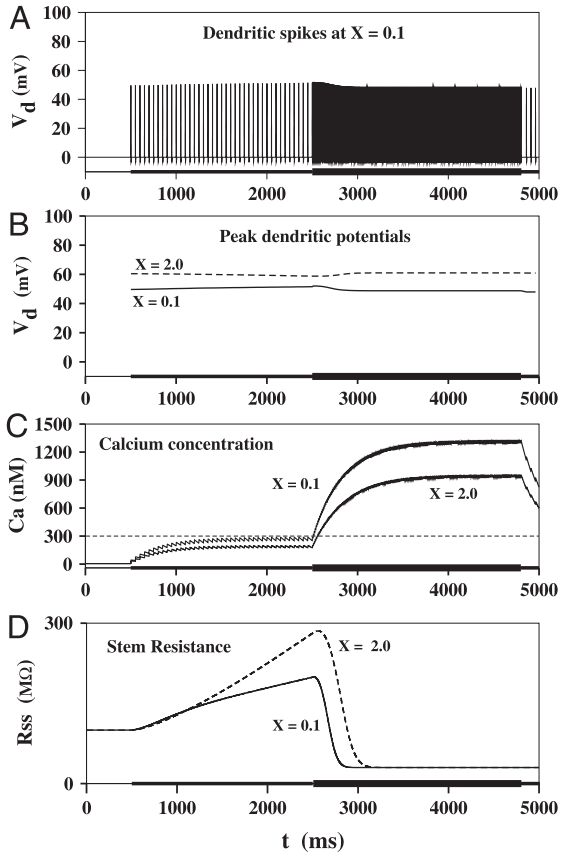

FIG. 18. At high spine densities and low spine stem resistance, high-frequency stimulation causing spine shortening has minimal effect on dendritic output. Here, the spine density is set to 35 and initially $R_{SS} = 100$ MΩ. Now R_{min} and R_{max} are reduced to 30 and 500 MΩ, respectively. These values of R_{SS} are consistent with recent experimental estimates (Tsay and Yuste 2004). Other parameters are the same as Fig. 17. *A*: amplitudes of dendritic potentials, at $X = 0.1$, do not decrease with the onset of high-frequency stimulation. *B*: peak dendritic potentials at the target, $X = 2.0$, exceed the peak potentials at $X = 0.1$ and $X = 0.4$. *C*: onset of high-frequency input pushes the calcium levels above C_{crit} along the entire branch. *D*: spine stem resistance drops to near 30 MΩ all along the branch because of the high calcium concentrations. Low stem resistances do not increase the threshold for action potential generation as was the case in Fig. 16, so there is no detrimental effect on the amplitude of the dendritic output.

Recently it has become clear that spine density and spine shape can change with remarkable rapidity in response to synaptic input. There is evidence that new spinelike structures can form in clusters between established spines (Harris et al. 2003) and that this is an ongoing process, such that in adult mouse cortex only about 50% of the spines are stable over a period of a month, with the remainder persisting for only a few days, even though the overall density only increases or decreases by an average of 1 spine/10 microns (Trachtenberg et al. 2002). Even though it is not yet certain as to the mechanisms underlying these changes, it is clear that local changes in spine density do occur in some systems. The subsequent effects of these time-dependent morphological changes on the physiological properties of individual dendritic branches are generally not measurable directly. In these simulations we examined the possible effects of localized, activity-dependent density increases, and spine stem shortening and lengthening, on neighboring unstimulated spines and on the output of the dendritic branch.

In the first set of simulations we model situations in which spines can extend from the dendrite and form new synapses adjacent to innervated spines as a result of activity in the latter group, thus increasing the local density. Under circumstances in which activity caused a local increase in the density of passive spines, there was a negligible effect of the addition of small numbers of new spines on the output of the dendritic branch. As has been previously demonstrated, in the absence of voltage-gated channels in either the dendrites or the spines, the electrotonic decay of potential along the segments of a dendritic tree is substantial (Segev and Rall 1988). However, in our simulation an addition of a few spines gave rise to a 2–3 mV increase in the amplitude of the electrotonically spread potentials into the neighboring spines such that any synchronous input from a separate pathway to the neighbors would be enhanced. The enhancement could come about either directly, by addition of the two potentials, or by a secondary effect. For example, depolarization is required to release *N*-methyl-D-

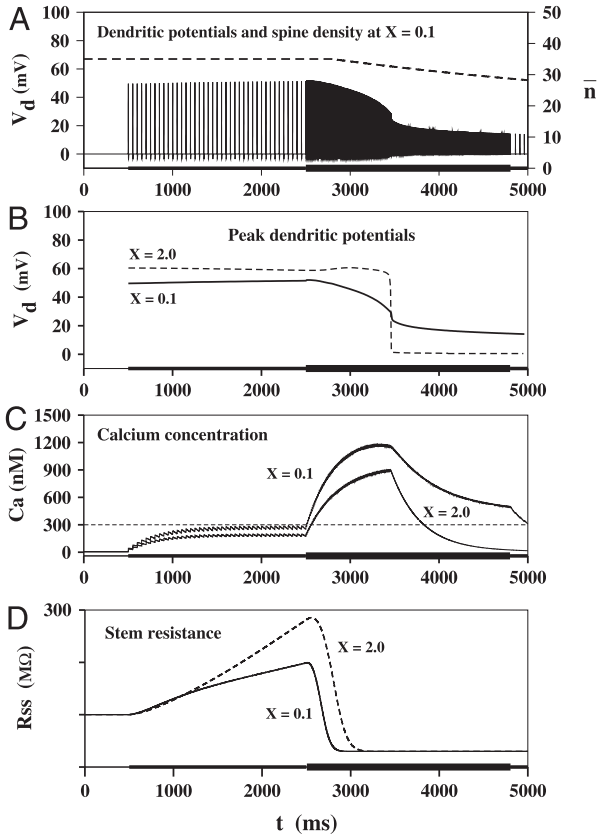

FIG. 19. Effects of stimulation-induced spine loss. An additional equation (*Eq. 15*), for a dynamic density $\bar{n}$, is added to the system of *Eqs. 11–14* to incorporate dendritic pruning if $R_{ss} < R^*_{ss}$ and $C_a > C_{crit}$. In the new equation $\bar{n}_{min} = 16$, $R^*_{ss} = 40$ MΩ, and the rate constant $\epsilon_3 = 2 \times 10^{-4}$. Other parameters are identical to Fig. 18. *A*: spine density (dashed) in the middle of the input region ($X = 0.1$) begins to decrease shortly after the onset of high-frequency stimulation due to the stem resistance falling below 40 MΩ, whereas the calcium concentration is >300 nM. Gradual decrease in spine density reduces the density of excitable channels until an action potential can no longer be generated in the input region. *B*: peak dendritic potentials at $X = 0.1$ and the distal part of the dendrite $X = 2.0$. Propagating action potentials at the distal part of the dendrite have larger peak values than the action potentials in the input region. This reverses when propagation fails at $t = 3{,}500$ ms. After stimulation-induced spine loss in the stimulated region, there is an abrupt decrease in peak amplitudes in the distal region. *C*: calcium concentration and *D*: stem resistance at $X = 0.1$ and $X = 2.0$.

aspatate channels from Mg^{2+} block, to allow them to respond to synaptic input from their innervating axons (Antonov and Johnson 1999; Nowak et al. 1984; Zhu and Auerbach 2001).

If activity was modeled to cause an increase in density, but all the spines were presumed to be active (have voltage-gated channels), the dendritic output rose gradually and then sharply as upstream spine densities reached levels that would support the propagation of an action potential. The rate of increase of output relative to the number of stimuli was sensitive to the spine stem resistance. At lower spine stem resistances, the rate of increase was slower, and provided a circumstance in which, for each successive input after an initial train, the output would be slightly larger over a long series of inputs. This would allow the dendritic branch to function essentially as a spike counter over this range, and the output would closely resemble that described as long-term potentiation, but would be derived from a change in the properties of the branch as a whole rather than of individual synapses.

In another scenario, synaptic input was assumed to increase intraspine calcium concentrations, and intraspine calcium concentrations were assumed to induce spine stem resistance through a change in length. The simulation allowed for spine stem elongation at modest Ca^{2+} concentrations, but if Ca^{2+} reached a critical level, the spine would collapse, as might be expected under conditions of excess calcium. It has not been possible to experimentally measure exact spine stem resistances, but we have some information as to the extremes of the range. Spine stem resistances could range from 30 MΩ (as calculated from the simple dimensions) to an upper boundary (estimated from the observed synaptic conductance) of 20,000 MΩ, although the latter is probably unrealistically high (Tsay and Yuste 2004). Neither of these methods takes into account the possibility that spines can change shape, losing or gaining constrictions, or losing or gaining an occluding structure such as a spine apparatus. Momentary constrictions or occlusions would increase spine stem resistance over the short haul, and would certainly be additional mechanisms that could be influenced by intraspine calcium concentrations besides length.

In passive spines, at modest stimulation frequencies such that calcium did not reach the critical level in the stimulated spines, the effect of spine lengthening did not significantly affect the amplitude of the dendritic output. On the other hand, if the dendritic branch was assumed to have active spines, as stimulation increased calcium levels and spine stem resistance, the effectiveness of the voltage-gated channels was enhanced. Neighboring spines received an enhanced signal and the output of the dendrite was substantially increased, as more and more spines were able to reach threshold for action potential generation. Interestingly, the starting spine stem resistance again determined the rate of increase of the dendritic output. When spines were assumed to be shorter, with lower R_{ss}, the slope of the increase over the critical region was less steep, leading to a much longer range of inputs that would give gradually increasing amplitudes of the outputs. Lower spine stem resistances favor a longer period over which the dendritic branch output is a function of the number of stimuli by a particular pathway. One could imagine a number of circumstances under which this would be a useful property in the nervous system. The scenario we modeled, which assumes that spine shapes remain elongated after they have been stimulated, fits with ideas suggesting that spine shape changes might be associated with learning (Lamprecht and LeDoux 2004). Furthermore there are stimulation frequencies with this model and its associated parameters that give rise to new stable spine stem resistances other than R_{max} or R_{min}. This suggests the possibility that under similar circumstances average spine neck lengths may reflect average frequencies of synaptic input.

Facilitation and long-term potentiation are generally thought of as an increase in the amplitude of the response generated at a particular synapse, and can depend on changes in either presynaptic or postsynaptic properties. However, the processes described above, where the dendritic output from a cluster of synapses is enhanced because of increased excitability of the branch, either through increase in spine density or increase in spine stem length, might also be thought of as a form of long-term potentiation. In this case, however, the changes additionally lead to an increase in the amplitude of the output if input were to occur on neighboring spines, and would also lead to an increase in the likelihood of back-propagated action potentials.

Such increases in the local excitability with LTP of a specific region of a dendrite have been seen in pyramidal neurons. After 40 min of bursting input, back-propagating action potentials and excitatory postsynaptic potentials (EPSPs) were increased in amplitude, and the Ca^{2+} influx associated with the back-propagating action potentials was enhanced near the synaptic input (Frick et al. 2004). In this case the mechanism was a localized enhancement of the A-type K^+ channels.

In this study we found very different effects of changes in spine density or spine shape, depending on whether voltage-gated channels were present in the spines. It is clear experimentally that some dendritic trees do conduct action potentials and have multiple kinds of voltage-gated channels, although often the exact distributions and types are not yet known. In our simulations we considered the case where the channels were clustered only in the spines as a starting point, and for computational simplicity. However, there is evidence that voltage-gated channels do occur more densely in the spine membrane than in the dendritic shaft (Frick et al. 2004; Hanson et al. 2004). Simulations have shown that such channel clustering is necessary for the conduction of action potentials, given the total numbers of channels thought to be present (Tsay and Yuste 2002).

When very high stimulus frequencies were used, calcium concentrations reached what was modeled to be a "critical" level, and spines were then caused to shorten drastically as suggested by Harris (1999). With certain parameters a similar effect was observed in these simulations. For very low stem resistance values, consistent with recent estimates by Tsay and Yuste (2004) and sufficiently large spine densities, action potential generation and propagation persist, in spite of the shape change because of clustered voltage-gated channels. However, in a scenario described by Müller et al. (1993), induced epileptic seizures and concomitant very high levels of activity caused both neuron death and loss of spines from surviving dendrites. This was accompanied by a reduction in evoked EPSP amplitudes. Spine loss with high-frequency stimulation was modeled as being caused by supercritical levels of

calcium and subsequent shortening of the spine below a critical length. When an activity induced spine loss was modeled, spines in the stimulated region were gradually lost at high-frequency stimulation. This resulted in an abrupt cessation of output from the dendritic branch when a little more than half the spines were gone. This kind of phenomenon would have a protective effect on downstream processes.

Because of the prevalence of dendritic trees that are capable of conducting action potentials, there is growing interest in the impact of back-propagating action potentials on the properties of the dendrite and spines (Golding et al. 2001; Tsay and Yuste 2002). In the presence of voltage-gated calcium channels, action potentials from any source, either forward or backward propagating, have the potential to change spine properties by calcium-dependent second messengers as effectively as input by the synapse. Thus in systems with voltage-sensitive spine properties, back-propagating action potentials have the potential to change the properties of many parts of the dendritic tree.

Enhancing spine density or spine stem resistance above critical levels leading to excitability can have more than just local effects. The utility of this kind of simulation is to uncover time-dependent changes that might be considered when thinking about the properties of the nervous system. The changes in output that we have observed, such as slow increases in the output as a function of number of input stimuli, are often attributed primarily to changes at the synaptic level. These simulations suggest that it would also be useful to consider small changes in the morphology of subsets of branches when considering plasticity.

ACKNOWLEDGMENTS

S. M. Baer gratefully acknowledges A. Bayliss, Dept. of Engineering Sciences and Applied Mathematics, Northwestern University, for introducing the numerical method used in this paper.

GRANTS

This research was supported in part by DMS-9320597 Grant, and D. W. Verzi was supported in part by Research Training Group Grant DBI-9602226 and faculty grant-in-aid 242122 from San Diego State University.

REFERENCES

Alonso G and Widmer H. Clustering of Kv4.2 potassium channels in postsynaptic membrane of rat supraoptic neurons: an ultrastructural study. *J Neurosci* 77: 617–621, 1997.

Annis CM, O'Dowd DK, and Robertson RT. Activity-dependent regulation of dendritic spine density on cortical pyramidal neurons in organotypic slice cultures. *J Neurobiol* 25: 1483–1493, 1994.

Antonov SM and Johnson JW. Permeant ion regulation of *N*-methyl-D-aspartate receptor channel block by Mg^{2+}. *Proc Natl Acad Sci USA* 96: 14571–14576, 1999.

Baer SM and Rinzel J. Propagation of dendritic spikes mediated by excitable spines: a continuum theory. *J Neurophysiol* 65: 874–890, 1991.

Dailey ME and Smith SJ. The dynamics of dendritic structure in developing hippocampal slices. *J Neurosci* 16: 2983–2994, 1996.

Engert F and Bonhoeffer T. Dendritic spine changes associated with hippocampal long-term synaptic plasticity. *Nature* 399: 66–70, 1999.

Fischer M, Kaech S, Knutti D, and Matus A. Rapid actin-based plasticity in dendritic spines. *Neuron* 20: 847–854, 1998.

Frick A, Magee J, and Johnston D. LTP is accompanied by an enhanced local excitability of pyramidal neuron dendrites. *Nat Neurosci* 7: 126–135, 2004.

Golding NL, Kath WL, and Spruston N. Dichotomy of action-potential backpropagation in CA1 pyramidal neuron dendrites. *J Neurophysiol* 86: 2998–3010, 2001.

Golding NL and Spruston N. Dendritic sodium spikes are variable triggers of axonal action potentials in hippocampal CA1 pyramidal neurons. *Neuron* 21: 1189–1200, 1998.

Gonzalez-Burgos G and Barrionuevo G. Voltage-gated sodium channels shape subthreshold EPSPs in layer 5 pyramidal neurons from rat prefrontal cortex. *J Neurophysiol* 86: 1671–1684, 2001.

Halpain S, Hipolito A, and Saffer L. Regulation of F-actin stability in dendritic spines by glutamate receptors and calcineurin. *J Neurosci* 18: 9835–9844, 1998.

Hanson JE, Smith Y, and Jaeger D. Sodium channels and dendritic spike initiation at excitatory synapses in globus pallidus neurons. *J Neurosci* 24: 329–340, 2004.

Harris KM. Calcium from internal stores modifies dendritic spine shape. *Proc Natl Acad Sci USA* 96: 12213–12215, 1999.

Harris KM, Fiala JC, and Ostroff L. Structural changes at dendritic spine synapses during long-term potentiation. *Philos Trans R Soc Lond B Biol Sci* 358: 745–748, 2003.

Harris KM and Stevens JK. Dendritic spines of CA 1 pyramidal cells in the rat hippocampus: serial electron microscopy with reference to their biophysical characteristics. *J Neurosci* 9: 2982–2997, 1989.

Helmchen F, Svoboda K, Denk W, and Tank DW. In vivo dendritic calcium dynamics in deep-layer cortical pyramidal neurons. *Nat Neurosci* 2: 989–996, 1999.

Hodgkin A and Huxley A. A quantitative description of membrane current and its application to conduction and excitation in nerve. *J Physiol* 117: 500–544, 1952.

Huguenard JR, Hamill OP, and Prince DA. Sodium-channels in dendrites of rat cortical pyramidal neurons. *Proc Natl Acad Sci USA* 86: 2473–2477, 1989.

Jonas P, Bischofberger J, Fricker D, and Miles R. Interneuron diversity series: fast in, fast out–temporal and spatial signal processing in hippocampal interneurons. *Trends Neurosci* 27: 30–40, 2004.

Jung HY, Mickus T, and Spruston N. Prolonged sodium channel inactivation contributes to dendritic action potential attenuation in hippocampal pyramidal neurons. *J Neurosci* 17: 6639–6646, 1997.

Kaech S, Parmar H, Roelandse M, Bornmann C, and Matus A. Cytoskeletal microdifferentiation: a mechanism for organizing morphological plasticity in dendrites. *Proc Natl Acad Sci USA* 98: 7086–7092, 2001.

Knott GW, Quairiaux C, Genoud C, and Welker E. Formation of dendritic spines with GABAergic synapses by whisker stimulation in induced adult mice. *Neuron* 34: 265–273, 2002.

Korkotian E and Segal M. Fast confocal imaging of calcium released from stores in dendritic spine. *Eur J Neurosci* 10: 2076–2084, 1998.

Korkotian E and Segal M. Release of calcium from stores alters the morphology of dendritic spines in cultured hippocampal neurons. *Proc Natl Acad Sci USA* 96: 12068–12072, 1999.

Krucker T, Siggins GR, and Halpain S. Dynamic actin filaments are required for stable long-term potentiation (LTP) in area CA1 of the hippocampus. *Proc Natl Acad Sci USA* 97: 6856–6861, 2000.

Kuske R and Baer SM. Asymptotic analysis of noise sensitivity in a neuronal burster. *Bull Math Biol* 64: 447–481, 2002.

Lamprecht R and LeDoux J. Structural plasticity and memory. *Nat Rev* 5: 45–54, 2004.

Magee JC and Johnston D. Characterization of single voltage-gated Na^+ and Ca^{2+} channels in apical dendrites of rat CA1 pyramidal neurons. *J Physiol* 487: 67–90, 1995.

Maletic-Savatoc M, Malinow R, and Svoboda K. Rapid dendritic morphogenesis in CA1 hippocampal dendrites induced by synaptic activity. *Science* 283: 1923–1927, 1999.

Müller D, Toni N, and Buchs PA. Spine changes associated with long-term potentiation. *Hippocampus* 10: 596–604, 2000.

Müller M, Gähwiler A, Rietschin L, and Thompson SM. Reversible loss of dendritic spines and altered excitability after chronic epilepsy in hippocampal slice cultures. *Proc Natl Acad Sci USA* 90: 257–261, 1993.

Nimchinsky EA, Sabatini BL, and Svoboda K. Structure and function of dendritic spines. *Annu Rev Physiol* 64: 313–353, 2002.

Nowak LM, Ascher P, Bregestovski P, Herbet A, and Prochiantz A. Voltage dependence of 1-glu induced current is due to gating by Mg ions. *Biophys J* 45: A388–A388, 1984.

Oliva AA Jr, Lam TT, and Swann JW. Distally directed dendrotoxicity induced by kainic acid in hippocampal interneurons of green fluorescent protein-expressing transgenic mice. *J Neurosci* 22: 8052–8062, 2002.

Segal M, Korkotian E, and Murphy DD. Dendritic spine formation and pruning: common cellular mechanisms? *Trends Neurosci* 23: 53–57, 2000.

Segev I and Rall W. Computational study of an excitable dendritic spine. *J Neurophysiol* 60: 499–523, 1988.

Svoboda K. Optical studies of single synapses in brain slices. *Biophys J* 76: A142, 1999.

Svoboda K, Tank DW, and Denk W. Direct measurement of coupling between dendritic spines and shafts. *Science* 272: 716–719, 1996.

Toni N, Buchs PA, Nikonenko I, Bron CR, and Müller D. LTP promotes formation of multiple spine synapses between single axon terminal and a dendrite. *Nature* 403: 421–425, 1999.

Trachtenberg JT, Chen BE, Knott GW, Feng GP, Sanes JR, Welker E, and Svoboda K. Long-term in vivo imaging of experience-dependent synaptic plasticity in adult cortex. *Nature* 420: 788–794, 2002.

Tsay D and Yuste R. Role of dendritic spines in action potential backpropagation: a numerical simulation study. *J Neurophysiol* 88: 2834–2845, 2002.

Tsay D and Yuste R. On the electrical function of dendritic spines. *Trends Neurosci* 27: 77–83, 2004.

Verzi DW. *A Mathematical Description of Diagrammatic Models for Structural Changes in Dendritic Spines* (PhD thesis). Claremont, CA: Claremont Graduate University, 2000.

Verzi DW and Baer SM. Calcium-mediated spine stem restructuring. *Math Comput Model* In press.

Wu HY and Baer SM. Analysis of an excitable dendritic spine with an activity-dependent stem conductance. *J Math Biol* 36: 569–592, 1998.

Zhu YL and Auerbach A. Na^+ occupancy and Mg^{2+} block of the *N*-methyl-D-aspartate receptor channel. *J Gen Physiol* 117: 275–285, 2001.